

University of Windsor

Scholarship at UWindor

Electronic Theses and Dissertations

Theses, Dissertations, and Major Papers

1-1-2006

A study of turbulence in open channel flow.

Bushra Afzal

University of Windsor

Follow this and additional works at: <https://scholar.uwindsor.ca/etd>

Recommended Citation

Afzal, Bushra, "A study of turbulence in open channel flow." (2006). *Electronic Theses and Dissertations*. 7064.

<https://scholar.uwindsor.ca/etd/7064>

This online database contains the full-text of PhD dissertations and Masters' theses of University of Windsor students from 1954 forward. These documents are made available for personal study and research purposes only, in accordance with the Canadian Copyright Act and the Creative Commons license—CC BY-NC-ND (Attribution, Non-Commercial, No Derivative Works). Under this license, works must always be attributed to the copyright holder (original author), cannot be used for any commercial purposes, and may not be altered. Any other use would require the permission of the copyright holder. Students may inquire about withdrawing their dissertation and/or thesis from this database. For additional inquiries, please contact the repository administrator via email (scholarship@uwindsor.ca) or by telephone at 519-253-3000ext. 3208.

A STUDY OF TURBULENCE IN OPEN CHANNEL FLOW

by

Bushra Afzal

A Thesis

Submitted to the Faculty of Graduate Studies and Research
through the Department of Civil and Environmental Engineering
in Partial Fulfillment of the Requirements for
the Degree of Master of Applied Science at the
University of Windsor

Windsor, Ontario, Canada

2006

© 2006 Bushra Afzal



Library and
Archives Canada

Bibliothèque et
Archives Canada

Published Heritage
Branch

Direction du
Patrimoine de l'édition

395 Wellington Street
Ottawa ON K1A 0N4
Canada

395, rue Wellington
Ottawa ON K1A 0N4
Canada

Your file Votre référence

ISBN: 978-0-494-35925-9

Our file Notre référence

ISBN: 978-0-494-35925-9

NOTICE:

The author has granted a non-exclusive license allowing Library and Archives Canada to reproduce, publish, archive, preserve, conserve, communicate to the public by telecommunication or on the Internet, loan, distribute and sell theses worldwide, for commercial or non-commercial purposes, in microform, paper, electronic and/or any other formats.

The author retains copyright ownership and moral rights in this thesis. Neither the thesis nor substantial extracts from it may be printed or otherwise reproduced without the author's permission.

AVIS:

L'auteur a accordé une licence non exclusive permettant à la Bibliothèque et Archives Canada de reproduire, publier, archiver, sauvegarder, conserver, transmettre au public par télécommunication ou par l'Internet, prêter, distribuer et vendre des thèses partout dans le monde, à des fins commerciales ou autres, sur support microforme, papier, électronique et/ou autres formats.

L'auteur conserve la propriété du droit d'auteur et des droits moraux qui protègent cette thèse. Ni la thèse ni des extraits substantiels de celle-ci ne doivent être imprimés ou autrement reproduits sans son autorisation.

In compliance with the Canadian Privacy Act some supporting forms may have been removed from this thesis.

Conformément à la loi canadienne sur la protection de la vie privée, quelques formulaires secondaires ont été enlevés de cette thèse.

While these forms may be included in the document page count, their removal does not represent any loss of content from the thesis.

Bien que ces formulaires aient inclus dans la pagination, il n'y aura aucun contenu manquant.


Canada

ABSTRACT

Three series of experiments were conducted to study the effect of Reynolds number, near-wall perturbation and background turbulence on the characteristics of smooth open channel flows. Measurements were carried out using a laser Doppler anemometer. The variables of interest include the mean velocity, the turbulence intensity, probability density distribution and Gram-Charlier series coefficients.

For the range of Reynolds number studied, the turbulence intensity profiles show that the effect of Reynolds number can be significant in open channel flows. However, the probability density distributions at various distances from the bed do not indicate any Reynolds number effects. The coefficients of the Gram-Charlier series expansion are nearly constant in overlap region and the region of nearly constant value of coefficients increase with increasing Reynolds number. The near-wall perturbed velocity profiles indicate that the overlap region develops more slowly than the inner and outer regions. The mean velocity profile is recovered at the farthest downstream station, whereas the turbulence intensity and higher-order coefficients do not indicate complete recovery. The presence of higher background turbulence significantly alters the characteristics of flow. Velocity defect in the outer region is decreased resulting in more negative values of the wake parameter, while the Gram-Charlier series coefficients are more uniformly distributed through out the depth.

ACKNOWLEDGEMENTS

I would like to express my profound appreciation and thanks to my advisor Dr. Ram Balachandar and Dr. Rupp Carriveau for their invaluable guidance, advice, inspiration, throughout insights, encouragement and support throughout my research on this thesis.

I would also like to offer my sincere thanks to my graduate committee members. I also thank Mr. M.A.A. Faruque for his support and assistance during my test runs.

Financial support from University of Windsor, and the Natural Science and Engineering Council are also greatly appreciated.

Thanks to my parents who have always supported me.

TABLE OF CONTENTS

ABSTRACT	iii
ACKNOWLEDGEMENTS.....	iv
LIST OF TABLES.....	vii
LIST OF FIGURES	viii
NOMENCLATURE	x
CHAPTER	
INTRODUCTION	1
1.1 Objectives	4
LITERATURE REVIEW	5
2.1 Reynolds number effects	5
2.2 Near-wall Perturbation	8
2.3 Background Turbulence	11
2.4 Power Law.....	13
2.5 Evaluation of Literature.....	15
EXPERIMENTAL SETUP AND PROCEDURES	17
RESULTS AND DISCUSSION	22
4.1 Mean Velocity profile	22
4.1.1 Reynolds number effect.....	22
4.1.2 Near-wall Perturbation	24
4.1.3 Background Turbulence	26
4.2 Turbulence intensity	28
4.2.1 Reynolds number effect.....	28
4.2.2 Near-wall Perturbation	30

4.2.3 Background Turbulence	31
4.3 Probability density distribution	31
4.3.1 Reynolds number effect.....	32
4.3.2 Near-wall Perturbation	33
4.3.3 Background Turbulence	33
4.4 Gram-Charlier Expansion Coefficients	34
4.4.1 Reynolds number effect.....	35
4.4.2 Near-wall Perturbation	36
4.4.3 Background Turbulence	36
4.5 Power Law	37
4.5.1 Reynolds number effect.....	37
4.5.2 Near-wall Perturbation	37
4.5.3 Background Turbulence	38
 CONCLUSIONS AND RECOMMENDATION FOR FUTURE WORKS	 54
5.1 Conclusions	54
5.1 Recommendations for future work.....	56
 REFERENCES	 57
 APPENDICES	
Appendix A: Uncertainty Analysis	65
 VITA AUCTORIS	 67

LIST OF TABLES

Table 1: Summary of Test conditions	23
-------------------------------------	----

LIST OF FIGURES

Figure 1:	Variation of wake parameter with Reynolds number based on depth of flow.	16
Figure 2:	Schematic of the flow field	20
Figure 3:	(a) Mean velocity profile in outer scaling & (b) inner scaling. (c) Velocity defect profile in outer scaling for various values of Reynolds number.	39
Figure 4:	(a), (b), (c) & (d) Mean velocity profiles downstream near-wall perturbation and undisturbed flow at various locations inner scaling. (e), (f), (g) & (h) mean velocity defect profile in inner scaling. (i), (j), (k) & (l) mean velocity profile in inner scaling using friction velocity from defect law.	40
Figure 5:	Mean velocity profiles for low and high background turbulence at various locations (a), (b), (c) & (d) outer scaling, (e), (f), (g) & (h) inner scaling. (i), (j), (k) & (l) Mean velocity defect profile.	41
Figure 6:	Distribution of Turbulence intensity in inner scaling for various values of Reynolds number (a) & (b) inner scaling (c) & (d) outer scaling.	42
Figure 7:	(a), (b), (c) & (d) Distribution of Turbulence intensity in inner scaling and undisturbed flow at various locations downstream of near-wall perturbation.	43
Figure 8:	Distribution of Turbulence intensity for high and low background turbulence at various locations.	44

Figure 9:	Probability density distribution of normalized u-component of velocity fluctuation.	45
Figure 10:	Probability density distribution of normalized u-component of velocity fluctuation downstream of near-wall perturbation and undisturbed flow.	46
Figure 11:	Probability density distribution of normalized u-component of velocity fluctuation for high and low background turbulence.	47
Figure 12:	Coefficients of Gram-Charlier expansion for various values of Reynolds number.	48
Figure 13:	Coefficients of Gram-Charlier expansion series at various locations downstream of near-wall perturbation and undisturbed flow.	49
Figure 14:	Coefficients of Gram-Charlier expansion series at various locations for high and low background turbulence.	50
Figure 15:	(a), (b) & (c) Power law Velocity profile for various values of Reynolds number. (d) & (e) Variation of Power law coefficients with Reynolds number based on depth of flow.	51
Figure 16:	Power law velocity profile for undisturbed flow and downstream of near-wall perturbation and undisturbed flow at various locations	52
Figure 17:	Power law velocity profile for low and high background turbulence at various locations..	53

NOMENCLATURE

ACRONYMS

2-D = Two-dimensional

LDA = Laser Doppler Anemometer

r.m.s = root mean square

ENGLISH SYMBOLS

B = log-law parameter (= 5.0)

C = power law parameter

C_f = skin friction coefficient

d = diameter of sphere

F_u = flatness

g = acceleration of gravity

h = depth of flow

H = shape parameter

Re_h = Reynolds number based on depth of flow

Re_θ = Reynolds number based on momentum thickness Reynolds number

S_u = Skewness

U = mean velocity in the x-direction

U_e = Maximum average velocity

u = instantaneous velocity at any point in the x-direction

U_τ = friction velocity

$U_{\tau D}$ = friction velocity from defect law.

U^+ = velocity in inner coordinate (velocity scaled by the friction velocity) = $U_{\tau} y/\nu$

u^+ = turbulence intensity = u/U_{τ}

x = location measurement down the length of the channel

y = location measurement through depth of the channel

y^+ = depth in inner coordinates (or depth scaled by friction velocity) = $y U_{\tau} / \nu$.

GREEK SYMBOLS

α = Power law parameter

δ = boundary layer thickness

δ^* = displacement thickness

κ = Von Karman constant

μ = viscosity of the fluid

ν = kinematic viscosity of the fluid

Π = wake strength parameter

θ = momentum thickness

ρ = fluid density

σ = standard deviation of velocity measurement

CHAPTER 1

INTRODUCTION

Similar to turbulent boundary layers, the velocity distribution in smooth open channel is divided into an inner and outer region. The two regions have distinct sets of characteristic velocity and length scales. In the viscous sublayer layer, the friction velocity $U_\tau = (\tau_w/\rho)^{1/2}$, is the appropriate scale, and the characteristic length scale is ν/U_τ . Here, τ_w is the wall shear stress and ν is the kinematic viscosity of the fluid. The viscous sublayer is mathematically described by $U^+ = y^+$, where $U^+ = U/U_\tau$, $y^+ = yU_\tau/\nu$, and y is the distance measured from the bed. A majority of the experimental evidence in open channel flow (OCF) supports the existence of a region near the wall where the velocity profiles scale logarithmically. Steffler et al., (1985), Nezu and Rodi (1986), Balachandar et al., (2002) have shown that there is an overlap layer ($30 \leq y^+ \leq 0.2hU_\tau/\nu$), where the mean velocity profiles agree well with the classical log-law given by:

$$U^+ = \frac{1}{\kappa} \ln y^+ + B \quad (1)$$

Here, $\kappa \approx 0.41$ and $B \approx 5$ are considered to be universal constants. The velocity distribution in the OCF farther from the wall ($y/h > 0.2$) is not expected to be affected by viscosity and the characteristic velocity scale is defined by the maximum velocity, U_e near the free surface, while characteristic length scale is the depth (h) of flow. In the outer region of the turbulent boundary layer (TBL) where the flow is mainly controlled by turbulence, Coles (1956) proposed a velocity defect law:

$$U_e^+ - U^+ = -\frac{1}{\kappa} \ln\left(\frac{y}{\delta}\right) + \frac{2\Pi}{\kappa} \cos^2\left(\frac{\pi}{2} \frac{y}{\delta}\right) \quad (3)$$

The non-dimensional quantity, Π , is called the wake parameter and is a measure of the deviation of the velocity distribution from the log-law. In the above equation δ is the

boundary layer thickness. For zero pressure gradient smooth TBL, Coles found that Π is 0.55 at high Reynolds numbers. In dealing with velocity profiles in the outer region of smooth OCF, Nezu and Rodi (1986) have noted that Π is dependent on Reynolds number. Cardoso et al., (1989) noted that values of Π varied from -0.27 to +0.2 in smooth, uniform open channel flow. Kirkgoz and Ardichoglu (1997) have also indicated very low values of Π (~ 0.1). Krogstad et al., (1992) proposed the following equation:

$$U_e^+ - U^+ = \frac{2\Pi}{\kappa} \left[1 - \frac{1}{2\Pi} \left(1 + 6\Pi \left(\frac{y}{\delta} \right)^2 - (1 + 4\Pi) \left(\frac{y}{\delta} \right)^3 \right) \right] - \frac{1}{\kappa} \ln \frac{y}{\delta} \quad (4)$$

The above equation has also been adopted for use in OCF (Balachandar et al., 2001 and Tachie et al., 2000). Tachie et al., (2003) have shown that the value of Π also depends on the roughness condition. The value of Π is also expected to be dependent on the level of background turbulence present in the flow.

Though analogies exist between TBL and flow in open channels, there are important differences which arise due to the presence of free surface and the channel side walls (Nezu 2005, Roussinova et al., 2006). The effect of the side walls is somewhat reduce when the aspect ratio (= channel width/flow depth) is large. Previous studies have indicated that the effect of the bed on turbulence is confined to a region close to the wall, whereas there is strong evidence that eddies are transported to the outer region. Nezu and Nakagawa (1993) have noted that the bursting motions in the inner layer interact with eddies formed in the outer layer. Only the stronger bursting motion near the wall can produce and sustain eddies in the outer region. This is supported by the fact that the period of the bursting motion at the wall coincides with the period of the boils formed at the free surface.

Even with the development of high speed computers, the use of direct numerical simulation is still limited and predictive methods continue to use turbulence models. The dependence on experimental data to formulate and validate such models has also continued. Because of the difficulty to achieve a fully developed, very high Reynolds number open channel flow under subcritical conditions, one needs to resort to working at lower Reynolds numbers. To this end, the dependence of the mean and turbulence parameters on the flow Reynolds number was studied for $Re_h = U_\epsilon h/\nu$ ranging from 23,000 to 72,000. It is also useful to study the response of the velocity profile to changing boundary conditions. The response of the velocity profile to a near-wall perturbation and changing turbulence levels in the flow were studied. The variables of interest include the mean velocity, probability density distribution of the velocity fluctuations and the Gram-Charlier series coefficients. The usefulness of the power law and the dependence of the power law coefficients on the flow conditions were also evaluated.

OBJECTIVES:

The purpose of this research is to further study the characteristics of turbulence in an open channel flow. The specific objectives are:

1. To study the dependence of the flow parameters on Reynolds number.
2. To examine the recovery of flow downstream of a near-wall perturbation.
3. To identify the applicability of power law in open channel flow.
4. To determine the effects of background turbulence on mean velocity distribution, probability density distribution and Gram-Charlier series coefficients.

To this end, variables of interest include the mean velocity, probability density distribution of the velocity fluctuations and examination of the Gram-Charlier series coefficients.

CHAPTER 2

LITERATURE REVIEW

In relation to the four objectives stated objectives in chapter 1, the literature review is also presented in four sections (2.1 to 2.4).

2.1 Reynolds number effects

In OCF literature, the values of the Reynolds number investigated are lower than those encountered in practice. It is therefore important to understand the usefulness of the results obtained from low Reynolds number experiments. The individual turbulence statistics obtained at different Reynolds numbers are expected to collapse on to a single curve when they are made dimensionless using proper scaling laws.

Purtell et al., (1981) investigated Reynolds number effects on a zero pressure gradient TBL over a range of momentum thickness (θ) Reynolds numbers $450 < Re_\theta = U_e \theta / \nu < 5100$. Their results showed that the overlap region did not disappear even at the lowest Reynolds number ($Re_\theta = 485$) examined. They observed that Π showed a distinct Re dependence for $Re_\theta < 2000$. In inner coordinates, the distribution of streamwise turbulence (u) was similar for $y^+ < 15$ while a much greater degree of similarity was noted when boundary layer thickness was used as the normalizing length scale.

Andreopoulos et al., (1984) studied Reynolds number effects in TBL for $3,624 < Re_\theta < 15,406$. The log-region showed the Karman constant (κ) to be independent of Reynolds number where as the constant B in equation (1) showed a slight decrease with

increasing Reynolds number. They also studied the probability density distribution of velocity fluctuations in the viscous sublayer and observed deviations from a typical Gaussian distribution for low Reynolds number flows. The deviation decreased at higher values of Re_θ .

Wei and Willmarth (1989) studied the effect of Reynolds number on turbulent channel flow in the range $2,970 < Re < 39,580$ (Here, Re is here based on centerline velocity and the channel half-width). The longitudinal turbulence intensity data scaled with inner variables, showed Reynolds number similarity up to $y^+ < 12$, but outside this range the data showed significant Reynolds number effects. The peak value of u^+ increased with increasing Re . The shear stress profiles also behaved in similar manner. The wall-normal turbulence intensity did not collapse using inner scaling at any distance from the wall. Wei and Willmarth (1989) indicated probe resolution errors became significant near the wall.

Durst et al., (1998) conducted measurements in a fully developed channel flow using a high resolution LDA. The Reynolds numbers (based on bulk velocity and channel width) varied from 2,500 to 9,800. They observed that the streamwise turbulence intensity scaled in inner variables for $y^+ \leq 50$. The peak value of the turbulence intensity was found to be 2.55 which was independent of Reynolds number.

Osaka et al., (1998) examined Re effects in a smooth wall TBL the in the range of $840 < Re_\theta < 6220$. They observed a reasonable collapse of the mean velocity in the

near-wall region. The magnitude of Π took on an asymptotic value of 0.62 when the Re was sufficiently high. The u^+ profiles showed Re independence for $y^+ \leq 20$ and peak values were found to be insensitive to Reynolds number.

Balachandar and Ramachandran (1999) conducted measurements in an open channel in the range of $180 < Re_\theta < 480$, and identified an overlap region where κ is independent of Reynolds number, and observed Π to decrease with increasing Re . The longitudinal mean velocity and turbulent velocity fluctuations showed similarity for the low values of Re_θ studied. The extent to which the data overlaps with the log-law decreased with decreasing Re_θ .

Tachie et al., (2003) conducted measurements in an OCF for Re_θ varying from 750 to 2400. The mean velocity profiles show that the extent of logarithmic region and Π increases with increase of Re . The turbulence intensities showed Reynolds number dependence for $y^+ > 30$ when inner scaling is used, but the profiles collapse reasonably well close to the wall and also in the outer region when outer scaling is adopted. The overlap region shows Re dependence, irrespective of the scaling used.

Balachandar et al., (2001) conducted an experimental study of TBL developing on smooth flat plate in an OCF ($800 < Re_\theta < 2900$). The skin friction coefficient was shown to decrease while the logarithmic region was found to increase with increasing Re_θ , while Π was found to decrease with increasing Re_θ . The peak value of the

turbulence intensity was shown to occur at $y^+ = 15$. The skewness of velocity fluctuations in streamwise direction was shown not to be constant and not equal to zero.

2.2 Near-wall perturbation

The flows subjected to sudden perturbation are encountered frequently in practice. For example, when offshore breezes encounter a coastline, the sudden change in surface roughness can have significant effect on the flow (Smits and Wood, 1985). Numerous papers and reviews have appeared on the influence of the perturbation and reorganization of a TBL. The types of perturbations include changes in surface roughness, boundary discontinuity, wall curvature etc. In assessing the degree of recovery or relaxation of the distorted flow towards the standard form, the structures of the two (i.e., the standard and recovering) flows are compared. The self-similarity in the log-law and the mean defect profile become useful criteria for the inner and outer regions, respectively. Some investigators have implied that a developing TBL is self-preserving if integral parameters such as the profile shape factor H , the momentum thickness θ , and the skin friction coefficient C_f become independent of streamwise distance. The critical aspect in the recovery process downstream of near-wall perturbation is, whether the inner layer or the outer layer that relaxes first to the standard form.

Smits and Wood (1985) conducted a review on the behavior of turbulent boundary layers subjected to sudden perturbations. They argued that the simplest possible perturbation is localized at the wall. The most common example is step change in roughness. The boundary layer responds to these perturbations by forming an internal

layer that is affected by the new boundary conditions. The outer layer response is particularly sensitive to the applied perturbation. If the downstream surface is rough, self preservation is quickly re-established, whereas if the downstream surface is smooth, the excess shear stress propagates across the layer and decays slowly toward self preservation.

Bushnell and McGinley (1989) indicate that the turbulence production process in wall bounded flows involve at least three different scales of motion. These are the outer large scales, which are of the order of boundary layer thickness, δ , intermediate scales with the characteristic dimensions of 100 wall units, and near-wall small-scale with characteristic dimensions of the order of 1~10 wall units. Because of the differences in the characteristic time and velocity scales in each region of the boundary layer, recovery process will depend on where the distortion is applied. Bushnell and McGinley (1989) implied that the relaxation process will be completed over a distance on the order of 100 length scales of the affected flow region. Thus, for a flow that is distorted in the outer region, recovery will be of the order of 100δ . For a boundary condition that primarily affects the inner layer (out of $y < 0.2\delta$), recovery will be on the order of 20δ .

Jung and Se (1992) conducted an experimental study to investigate a redeveloping turbulent boundary layer downstream of a backward facing step. In the region following reattachment, the mean velocity distribution slowly recovers to the form of an equilibrium boundary layer. During this process the flow in the inner region reaches

equilibrium rapidly, while the flow in the outer region experiences a much slower change.

Le et al., (1997) carried out a direct numerical simulation of a flow over a backward facing step and found that the velocity profiles deviated from the log-law even at 20 step heights following separation.

Castro and Epik (1998) conducted boundary layer measurements downstream of the highly turbulent separated flow generated at the leading edge of a blunt flat plate. They considered two cases: first, when there is only low (wind tunnel) turbulence present in the freestream flow and a second when rough isotropic homogeneous turbulence is introduced. They concluded that the development process is very slow and non-monotonic. They argued that as far as turbulence is concerned, the inner region develops no more quickly than the outer flow, and it is the latter which essentially determines the overall rate of development of the whole flow. By comparison with data obtained by other workers in different, but related flows, they mentioned that the features of the developing boundary layer are quantitatively independent of the precise nature of separation and reattachment process.

Tachie et al., (2001) conducted measurements of mean velocity and turbulence statistics upstream and downstream of a 3-mm forward facing step in a shallow open channel flow. They showed that the overlap region develops more slowly than the inner and outer regions. The mean profile recovers at $x/h > 100$ but the profiles do not collapse

onto the upstream profiles. They showed that the viscous sublayer was insensitive to the imposed disturbance and the recovery process, was more rapid and complete at $x/h = 10$. A reasonable agreement between the upstream and downstream mean velocity profile at $x/h \geq 50$ was observed. The streamwise turbulence intensity displayed two peaks immediately downstream of the reattachment location. The recovery process of turbulence intensity was much slower compared to the mean flow.

2.3 Background turbulence

Compared to a canonical boundary layer, open channel flows generally have higher levels of turbulence. Besides, there are many near-wall engineering applications where one needs to understand the role of background turbulence. For smooth wall boundary layers at elevated freestream turbulence Bradshaw (1978) argued that the log-law holds when there is local equilibrium in the near-wall region. Hancock and Bradshaw (1989) measured various terms in the turbulence energy transport equation at a turbulence intensity $Tu \leq 6\%$ and found the boundary layer to be in local equilibrium. Thole and Bogard (1996) extended the data to Tu values as high as 20%. Among other findings they confirmed the validity of log-law at high freestream turbulence and noted significant alterations of the outer region of the boundary layer. Based on the measured velocity spectrum, they found that at $Tu = 20\%$, the freestream turbulence penetrates deep into the near-wall region.

Hancock and Bradshaw (1983) conducted mean flow and turbulence measurements on a boundary layer beneath a nearly homogeneous isotropic grid

generated turbulent flow. They showed that as the freestream turbulence increases, the outer region of the boundary layer exhibits a depressed wake region. Hoffman and Mohammadi (1991) showed a decrease in the value of Π with increasing freestream turbulence level.

Balachandar and Tachie (2001) generated a high turbulent flow caused by the interaction between a boundary layer on a horizontal floor of a shallow open channel flow and the wake of a thin flat plate mounted vertically on floor of the channel. Their results indicate that the profiles in the near wake region are quite distorted and the recovery of the boundary layer to the upstream condition is slow. Their results also indicate that the inner region appears to develop more quickly than the outer flow. The velocity profiles indicate that the wake effects are prevalent at 200 plate widths downstream of wake generator. Neither mean nor higher-order moments indicate a complete recovery even at large distances from the turbulence generator.

Krampa-Morlu and Balachandar (2005) changed the turbulence levels in a smooth open channel by suspending a flat plate and examined recovery in terms of mean velocity, turbulence intensity and quadrant decomposition, and the results indicated that the near-wall region recovers faster than the outer region. They revealed that at the last measuring station, away from the wall region, the flow was still being influenced by the upstream disturbance.

Balachandar and Patel (2005) studied effect of near free surface disturbance imposed in an open channel flow in the presence of low and high background turbulence. The Π parameter and the normalized turbulence levels were reduced in the presence of high turbulence.

2.4 Power Law

The scaling law for the overlap region has been of considerable interest to the fluid dynamics community because it directly leads to skin friction laws. The specific form of the scaling law in the overlap region depends on the assumptions made in the course of the matching process. Depending on the specific assumptions implied, a log-law or a power law is obtained. The power law velocity profile is usually written as:

$$U^+ = Cy^{+\alpha} \quad (5)$$

The log-law assumes that the velocity gradient in the main body is independent of molecular viscosity, where as power law assumes that the velocity gradient of the main body of the flow remains dependent on viscosity up to some arbitrary large Reynolds number (Barenblatt and Prostokishin, 1993). Attempts have been made to use refined experimental data to identify the proper scaling law for the overlap region. The boundary layer measurements reported by Osterlund et al., (2000) provide evidence in support for a log-law; however, a reanalysis of the same data by Barenblatt (1993) suggests that the data are better described by a power law. Recent measurements at low Reynolds numbers and direct numerical simulation (DNS) results show that the overlap region gradually disappears as the Reynolds number decreases. This has important implications because

without a well-defined log-law region the usefulness of the Clauser plot technique to determine the skin friction is severely diminished.

2.5 Evaluation of Literature

The present literature review indicates that many interesting aspects related to mean velocity and turbulence have been resolved but several questions still need to be addressed (Smits and Wood, 1985). For example, the peak value of the turbulence intensity has been found to be independent of Re while others note a dependence on Re . There are differences in the variation of Π with Re . A sample plot of previous results for smooth OCF is shown in Figure 1. Clearly, the literature points to varying trends. The topic of interest in perturbed flows dealing with the recovery process is whether it is the inner layer or the outer layer that relaxes first to the standard form. Castro and Epik (1998) indicated that as the inner and outer layers are dynamically linked, the inner layer cannot possibly develop normally until the outer layer has become more normal. Tachie et al., (2001) argue that the recovery process depends on the flow parameters that are being examined. The present study aims to resolve some of the issues related to the near-wall perturbation, Reynolds number effect and background turbulence.

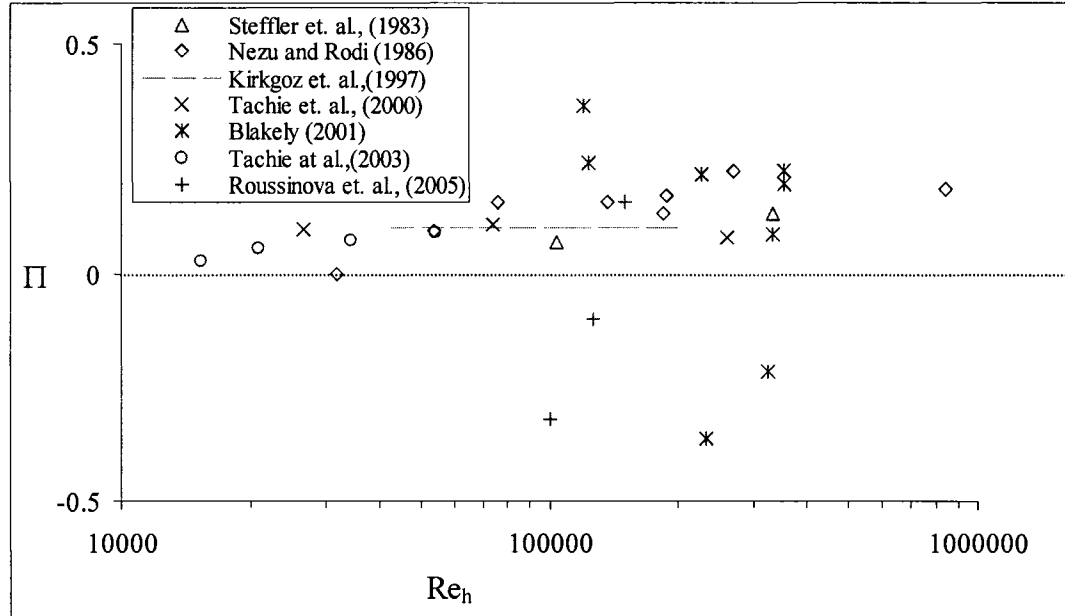


Figure 1: Variation of wake parameter with Reynolds number based on depth of flow

CHAPTER 3

EXPERIMENTAL SETUP AND PROCEDURES

The present experiments were conducted in a 9.5 m long, 1.2 m wide and 0.6 m deep rectangular cross section open channel flume having a recirculating flow system. The side walls and bottom of the flume are made of Plexiglas to facilitate unobstructed transmission of the laser beams. A tailgate was used to control the depth of flow. The flow was conditioned by using a flow straightner packed with plastic straws and located at the flume entrance. The depth of flow was constant in all tests at 100 mm. The corresponding aspect ratio of 12 is large enough to minimize the effect of secondary currents as the measurements were conducted along the flume axis (Muste and Patel, 1997). Measurements were carried at a streamwise distance of 5.25 m (or greater) downstream of the flume entrance (Figure 2). The Reynolds number of the flow based on the distance from the start of the flume varied from 1.1×10^6 to 3.7×10^6 . Sand particles were glued on to the bottom of the channel as a 25-mm wide strip spanning the entire width of the flume at 3.5 m downstream of the flume entrance. This additional effect of tripping ensured the attainment of a fully developed turbulent state.

Velocity measurements were conducted using a two-dimensional laser Doppler anemometry (LDA) system. The LDA was powered by 300 mW argon-ion laser. The optical system includes a Bragg cell, a beam expansion unit and a 500 mm focusing lens. The LDA system was operated in backward scatter mode. The measuring volume for the present configuration was $0.124 \times 0.123 \times 1.65 \text{ mm}^3$. The probe resolution in the wall

normal direction (in wall units) for present test conditions was $1.2 < l^+ < 3.4$, which is adequate enough to allow reliable measurements of both the mean velocity and turbulence intensity (Gad-el-Hak and Bandyopadhyay 1994). The LDA was set to obtain 10,000 velocity realizations or 1800 seconds of measurement at each point in the profile, whichever occurred first. The LDA probe was mounted on a two-dimensional computer controlled traversing system capable of attaining the same location with an accuracy of $\pm 0.01\text{mm}$. The water was filtered for several days prior to the start of the test and 5 micron diameter seed particles were added to the flow to facilitate velocity measurements. The LDA data rate varied from 10 Hz close to the wall to about 50 Hz at distances remote from the wall.

Three series of experiments were conducted. Series A was conducted on a hydraulically smooth surface at three different Reynolds numbers. Series B and Series C denoted the near-wall perturbation tests and the background turbulence tests, respectively. Series A test conditions are summarized in Table 1, where Tu denotes the turbulence intensity at the location where U_e is obtained and X denotes the distance from the start of the flume to the measurement station. In Series B, the near-wall perturbation was generated using a row of 5-mm diameter spheres glued to the bottom of the channel spanning the entire width of the flume. The row of spheres was located 5.25 m from the entrance to the flume. The velocity and depth of flow was kept constant at 0.38 m/s. Velocity measurements were made at four axial stations ($x/d = 10, 20, 40$ and 60) downstream of the spheres (here, x is as defined in Figure 2). A summary of the Series-B test conditions is also provided in Table 1. In this table, SM denotes smooth wall tests

without near-wall perturbation and NP denotes the perturbed flow. In Series C, the high background turbulence (denoted High-Tu) was generated by removing the flow straighter and the measurements were made at three stations (indicated as Stations A, B and C) separated by a distance of 100 mm between them. The first station (A) was located 5.35 m downstream of the flume entrance

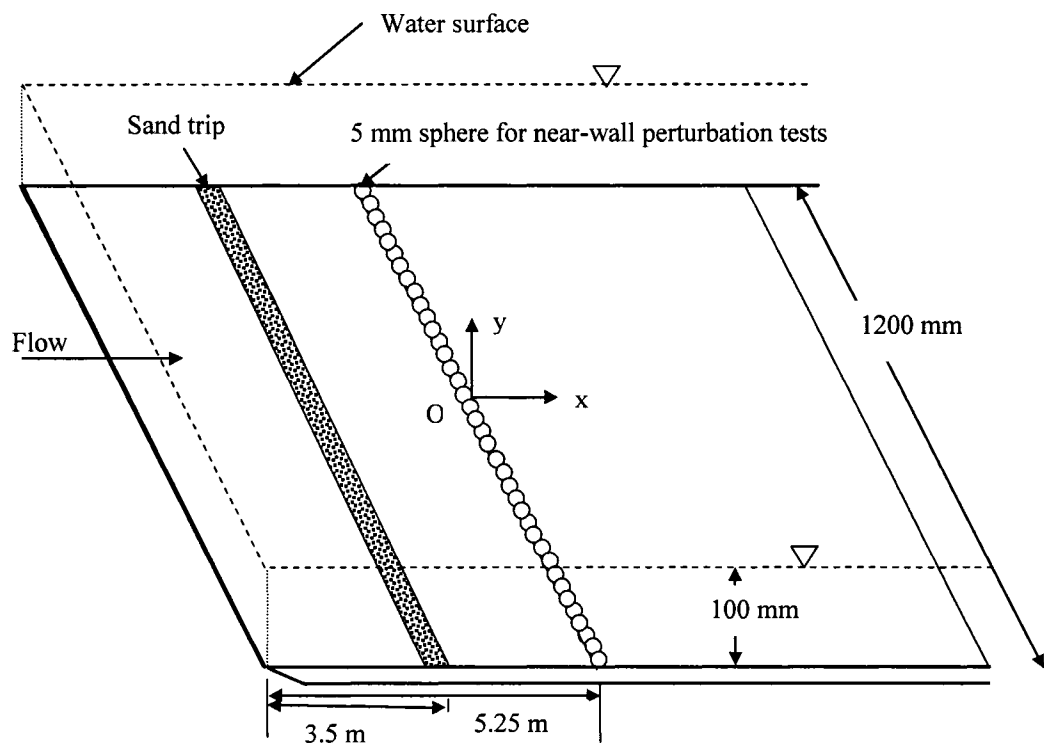


Figure 2: Schematic of the flow field

Table 1: Summary of Test conditions

Test		Location	U_e (m/s)	Tu (%)	Re_θ	Re_h
Reynolds number effect (Series A)						
A- Re_1		X = 5.45 m	0.559	4.10	5280	72,000
A- Re_2		X = 5.45 m	0.379	2.90	3540	49,214
A- Re_3		X = 5.45 m	0.199	3.20	1260	23,000
Near-wall perturbation (Series B)						
B-SM1		x/d =10	0.379	3.16	3357	49,214
B-SM2		x/d =20	0.379	3.16	3357	49,214
B-SM3		x/d =40	0.379	2.90	3540	49,214
B-SM4		x/d =60	0.379	3.44	3561	49,214
B-NP1		x/d = 10	0.379	3.59	3499	49,214
B-NP2		x/d = 20	0.379	4.19	3246	49,214
B-NP3		x/d = 40	0.379	4.19	3295	49,214
B-NP4		x/d = 60	0.379	3.37	3725	49,214
Background turbulence (Series C)						
Low-Tu	Station A	X = 5.35 m	0.379	3.16	3357	49,214
	Station B	X = 5.45 m	0.379	2.90	3540	49,214
	Station C	X = 5.55 m	0.379	3.44	3561	49,214
High-Tu	Station A	X = 5.35 m	0.379	5.16	2579	49,214
	Station B	X = 5.45 m	0.379	4.65	2736	49,214
	Station C	X = 5.55 m	0.379	4.86	2816	49,214

CHAPTER 4

RESULTS AND DISCUSSION

In accordance with the objectives of the present study, the role of Reynolds number, the effects of near-wall perturbation and background turbulence are analyzed. The mean aspects are considered first, which also serve to validate the measurement procedures used in the study. Following this, light is shed on velocity probability density distribution and Gram-Charlier series coefficients.

4.1 Mean velocity profiles

4.1.1 Reynolds number effect

The mean velocity profile in outer scaling along the centreline of the flow for the three tests is shown in Figure 3a. The wall normal distance (y) is normalized by the maximum flow depth (h), and the mean velocity (U) is normalized by the maximum value near the free surface (U_e). It can be seen that mean velocity profiles collapse reasonably with a slight Reynolds number dependence that is consistent with earlier observations in turbulent boundary layers (Schlichting, 1979). The mean velocity profiles in inner coordinates at the three Reynolds number are shown in Figure 3b. The friction velocity was evaluated from the velocity measurements by applying the log-law with $\kappa = 0.41$ and $B = 5$. As expected, the profiles collapse on to a single curve at the three Reynolds numbers. As Re increases, the extent over which the experimental data collapse onto the log-law increases. The extent, denoted as $l^+ = U_\tau l/\nu$, varies from $l^+ = 1088$ at A- Re_3 to $l^+ = 2940$ at A- Re_1 . It is thus possible that the wall and wake regions

approach each other and may finally overlap at a very low value of Re . The variation of skin friction coefficient C_f with Re_θ is shown as an inset in Figure 3a. Here, C_f is based on the U_τ obtained from Clauser chart. As expected, C_f shows a decreasing trend with increasing Re_θ . The present data trend compares favorably with the data of Tachie et al., (2003), Purtell et al., (1981) and Osterlund (1999). The present values of C_f are relatively higher than that obtained at similar Re_θ in a canonical TBL. As noted from literature and will be shown later, the higher values of C_f in open channel flows is due to the higher background turbulence intensity and the lower values of Π . The boundary layer shape parameter H defined as the ratio of displacement thickness to momentum thickness is plotted in the inset in Figure 3b, which varies from 1.27 to 1.29. The magnitude of H is similar to that reported in previous studies. The present data trends for C_f and H are indicators that the open channel flow data can be compared to standardized flows such as zero-pressure gradient turbulent boundary layers.

The velocity defect profiles are shown in Figure 3c, where U_e is used as the velocity scale. There is small systematic decrease in the mean velocity defect as Re_θ increases. Tachie et al., (2003) also showed a systematic decrease in the mean velocity defect as Re_θ increases. The velocity defect profile for a zero pressure gradient smooth flat plate TBL is also shown with $\Pi = 0.55$. Clearly the value of Π is not equal to 0.55 in open channel flow. This difference has been attributed to the free surface effect present in open channel flow and the elevated levels of background turbulence.

Following Tachie (2001), the values of friction velocity ($U_{\tau D}$) and Π were computed using equation (3) and the two parameter optimization procedure. The value of Π can also be computed using equation (3) and the value of U_{τ} obtained from the Clauser chart. The two estimates of Π are shown in the inset of Figure 3c. It should be noted that the difference in the shear velocity obtained by two parameter optimization procedure compared to that obtained using log-law is 10% for Test A-Re₁, $\pm 6\%$ for A-Re₂ and $\pm 3\%$ in A-Re₃.

Libby (1996) examined in detail the effect of the wake parameter in terms of different pressure gradients. His analysis shows that the deviation from logarithmic distribution applicable at outer edge of the boundary layer significantly increases as the adverse pressure gradient becomes stronger. Conversely, in favorable gradients the logarithmic law applies over most of the boundary layer thickness. The negative values of the wake parameter are physically possible for flows with favorable pressure gradients (accelerating flow). In the present experiments, since the bed slope is held constant, the pressure gradient should be favorable and close to zero. Thus it is expected that the value of the wake parameter will be negative.

4.1.2 Near-wall perturbation

The mean velocity profiles for Series-B are plotted in a three-column format in Figure 4. The distributions denoted by the solid diamonds refer to the velocity profile without the perturbation. In the first column, U_{τ} obtained from the Clauser chart is used as the velocity scale, while in the third column $U_{\tau D}$ evaluated from equation (3) is

utilized. The uncertainties in the estimation of U_τ is expected to be high as the overlap region is rather small, especially at $x/d = 10$. The computation of $U_{\tau D}$ assumes that the outer region is not significantly affected by the near-wall perturbation. In the first column, the profile at $x/d = 10$ is very much distorted due to the near-wall perturbation. The deviation from log-law in the outer region signifies that a strong wake component exists at $x/d = 10$. This is consistent with earlier results of Korgstad and Antonia (1992) and may suggest that there is a stronger coupling between the inner and outer layers, than that implied by Townsend's similarity hypothesis. As one moves farther from the disturbance, i.e., $x/d = 20$ and 40 , the length of the overlap region increases, and it can be said that the flow is recovering. At $x/d = 60$, the velocity profile collapses on to the reference profile over the entire flow, and the mean velocity profile has completely recovered. The insets in the first column show the velocity measurements closer to the wall in outer scaling. It can be noted that the deviations are the greatest in the region $0.05 \leq y/h \leq 0.15$ which corresponds to the overlap region. Balachandar and Tachie (2001) conducted measurements in a separated flow downstream of forward facing step and observed the largest deviation for $0.05 \leq y/h \leq 0.15$. They also noted that the relaxation process was non-monotonic and observed that the corresponding velocity gradient was higher than the reference profile for $x/d \leq 20$. The authors suspected that this may be due to higher entrainment of outer flow into the near-wall region at locations closer to the point of separation. In the present study, following separation of flow from the top of the spheres and reattachment on the bottom wall, one would expect the occurrence of complex turbulent mechanisms due to the unsteady nature of the reattachment zone leading to intense mixing and homogenization of the flow. The profiles in the last row

clearly indicate a fair amount of recovery to the reference condition. Based on the results of Bushnell and McGinley (1989), one would expect the flow to completely recover at a distance of $20h$ or $400d$. This indicates that at least in the mean sense, there has been a fairly quick recovery in the present study.

The middle column shows the defect profiles compared to the undisturbed flow. The outer region ($y/h > 0.2$) is very similar in both flows and $U_{\tau D}$ is expected to be the more appropriate representation of the friction velocity. One can note that the effect of the perturbation diminishes with increasing x/d but penetrates more into the overlap and outer region. The flow recovery is not complete at $x/d = 60$. From the third column of graphs, it is clear that the disturbance affects not only the overlap region but also the outer region.

Some investigators have implied that a developing TBL is self-preserving if integral parameters such as the profile shape factor (H) and the skin friction coefficient (C_f) become independent of the streamwise distance. The variation of C_f with x/d is shown in the inset of Figure 4e. Clearly, the flow is progressing towards recovery state and is far from reaching self-preservation.

4.1.3 Background turbulence

Figure 5 shows the mean velocity profiles at various stations for the low and high turbulence conditions. At all three stations, when the data is plotted in outer scaling (column 1), the mean velocities are slightly larger in the presence of high background

turbulence for $0.1 < y/h < 0.7$. A change in the level of turbulence does not affect the conformation of the data with log-law (column 2) and the estimated values of U_τ for the two turbulence conditions did not show significant differences at all three stations (see insets in Figure 5b and 5c). The extent of collapse of the data with log-law is shortened in the case of High-Tu. The overlap extent, l^+ varies from 1319 at Station A to 1490 at Station C for High-Tu, whereas at low turbulence, the corresponding values are 2020 and 2063, respectively. Further, for High-Tu, the velocity profile in the outer region falls below the log-law resulting in more negative wake parameters values. Thole and Bogard (1996) also made a similar observation in a TBL. In column 3, the effect of High-Tu can be noticed through out the depth. In this graph, $U_{\tau D}$ is used as the friction velocity. The computed values of Π are also shown in the insets in Figures 5b and 5c for Low-Tu and High-Tu, respectively. There are no significant differences between the shear velocities computed from the log-law and the two-parameter optimization of equation (3) for the Low-Tu tests. However, there are significant differences (of the order of 30%) between U_τ and $U_{\tau D}$ computed for the high turbulence flow.

The variation of C_f with turbulence intensity with the two levels of background turbulence is shown in the inset of Figure 5a. The skin friction coefficient is higher for higher Tu. The data of Hancock & Bradshaw (1983) and Hoffman & Mohammadi (1991) are also plotted in the inset and compares well with the present experimental data.

4.2 Turbulence intensity

4.2.1 Reynolds number effect

Figure 6a shows the turbulence intensity profiles at a nearly constant Reynolds number ($Re_0 \sim 1200$) including the OCF measurements by Tachie et al., (2003), the TBL measurements of Osaka et al., (1998) and Purtell et al., (1981), and the fully developed channel flows of Harder & Tiederman (1991). All the profiles collapse reasonably well in the near-wall region ($y^+ < 30$). Beyond $y^+ > 30$, the measurements in the open channel are consistently higher values than that of the standard boundary layer. This can attributed to the relatively higher background turbulence levels that usually occur in open channel flows. Figure 6b compares the u^+ profiles for the present experiments using inner variables for Series A. For these profiles some scatter appear in the near-wall region. This may be due to difficulty in determining the exact location of the wall ($y = 0$) and further complicated by measurement difficulties using the LDA in the region closest to the wall. The present data indicates that the peak value of u^+ is in the range 2.5 to 3 similar to the experimental data of Ching et al., (1995) and Purtell et al., (1981). The peak values of u^+ for the present profiles occur in the range of $10 < y^+ < 15$, this is where a transition occurs within the boundary layer from the inner viscous region to the turbulent inner region. The peak value of u^+ increases with increasing Re_0 which agrees well with the predictions of Spalart (1988), Purtell et al., (1981) and Wei & Willmarth (1989), where as Tachie et al., (2003) show that the peak value of u^+ occur in the range $13 < y^+ < 15$ irrespective of Re . Wei & Willmarth (1989) showed Reynolds number similarity up to $y^+ \leq 12$. Tachie et al., (2003) observed Reynolds number similarity for $y^+ \leq 30$, whereas Spalart (1988), Purtell et al., (1981) and Ching et al., (1995) indicate similarity for $y^+ < 15$. The present data

trend clearly indicates a strong Reynolds number effect. The intensity of turbulence drops as free surface is approached. A clear dependence on Re_θ is visible for $y^+ > 100$.

The distribution of streamwise turbulence intensity in outer variables is shown in Fig 6c. The profiles collapse well for $y/h > 0.2$ while Reynolds number effects are evident in the overlap region. The location of peak value of u/U_e reduces in magnitude as Re_θ increases. These observations are different from those noted in Figure 6b. This indicates that depending on the type of scaling chosen one can arrive at different conclusions. Figure 6d shows the streamwise turbulence intensity normalized by friction velocity and depth of flow normalized with depth of flow. Nezu and Nakagawa (1993) suggested an equation which describes a mean trend using mixed scaling. This is indicated as a line in Figure 6d.

Use of outer scaling successfully removes the effects of the Reynolds number from the outer flow. Similarly, U_τ as the velocity scale tends to remove the Re effects from the inner flow but not in the outer region. However, both outer scaling and classical scaling do not absorb the effect of Reynolds number in overlap region. The use of an intermediate scaling suggested by Roussinova et al., (2006) was attempted and is shown as an inset in Figure 6d. Barring the very near-wall region ($y^+ < 15$), this scaling absorbs Reynolds number effects.

4.2.2 Near-wall perturbation

The distribution of turbulence intensity in inner coordinates downstream of the near-wall perturbed flow and the undisturbed flow is shown in Figures 7a-7d. Here, $U_{\tau D}$ is used as the normalizing scale. In these graphs, line A-B denotes a horizontal line through the top of the spheres. The reference profile (B-SM) is similar to the OCF measurements of Tachie et al., (2000) at similar Reynolds number. In the perturbed flow, at $x/d = 10$, the peak value of u^+ is 5. For $x/d > 10$, there is a clear tendency to exhibit two local peaks. For example, at $x/d = 20$, the peaks and their corresponding locations are: $u^+ = 2.9$ at $y^+ = 12$ and $u^+ = 3.4$ at $y^+ \approx 100$. The experimental results of Tachie et al., (2001) with a different kind of near-wall perturbation also indicate two peaks in the region $10 \leq x/d \leq 20$. The DNS and LES results of Suksangpanomrung (1999) as well as the DNS (Le et al., 1997) and experimental (Jovic and Driver, 1994) results also indicate two peaks in the region $10 \leq x/d \leq 20$. Le et al., (1997) remarked that the turbulence structure in the recirculation region of a backward facing step, the turbulence transport term removes energy from the shear layer region and delivers it to the near-wall region. In the present study, the flow separation from the sphere reattaches to the bed and forms a mixing zone downstream of the reattachment point (see inset in Figure 7a). This is indicated by a region of very high turbulence in Figure 7a, and the two peaks (near-wall peak and mixing zone peak) are perhaps located very close to each other at $x/d = 10$. Due to the spreading of the mixing zone, at subsequent stations, the location of the peak moves away from the wall, while the magnitude of the peak decreases. Simultaneously, due to near-wall flow recovery, a well defined near-bed peak appears. This is similar to the near-wall peak in the unperturbed flow.

One may recall that the largest deviations in the mean velocity profiles from the reference profile are in the overlap region ($30 \leq y^+ \leq 200$). The u profiles also exhibit a similar behavior. The agreement between the reference profile and the perturbed flow (at $x/d = 60$) is reasonable in the inner and outer region. Similar to the velocity defect profile, turbulence intensity has not completely recovered in the overlap region.

4.2.3 Background turbulence

Figures 8a-8c show the effect of turbulence on the u profiles. The profiles at Stations A and B with High-Tu show higher value of turbulence intensity compared to that of Low-Tu. The difference in the turbulence intensity can be seen throughout the depth of flow. The three figures show that with increasing streamwise distance the effect of background turbulence decreases. At Station C, the two profiles collapse in the inner region where as the effect of background turbulence can be still observed in the outer region.

4.3 Probability Density Distribution

Up to this point, the average values of the fluctuating quantities were considered. In an effort to further understand the role of turbulence, the distributions of the fluctuations are now considered. In order to obtain probability density $p(u)$, the fluctuations are classified into bins and the use of a proper bin size to sort the data is required. In this study, the bin size is standardized at 0.2σ , where σ is the standard deviation.

4.3.1 Reynolds number effect

The $p(u)$ distribution at various values of y^+ is shown in Figure 9. A standard Gaussian distribution is also shown in each of the graphs. The $p(u)$ distributions close to the wall are negatively skewed and deviate from a Gaussian distribution due to intermittent nature of flow. Kline et al., (1967) have shown that the streaky structures dominate the flow near the wall region. These structures contribute to sweep and ejection type events which play a major role in the transport of mass, momentum, and energy in wall bounded flows. Compared to TBL, Roussinova et al., (2006) have noted that the strength of both sweeps and ejections is greater in OCF. The strong prevalence of ejections in the outer regions is another characteristic of OCF. Both types of events provoke the non-Gaussian character of the probability density distributions of the velocity fluctuations.

As we move farther away from the wall, the $P(u)$ distributions are closer to a Gaussian distribution in overlap region which compares well with the results of Tsuji and Nakamura (1999) and Durst et al., (1997). In this region, intense mixing and the resulting momentum exchange result in Gaussian distribution of velocity probability density distribution with skewness tending to zero. Dinavahi et al., (1995) also observed the self similarity of probability density distribution beyond the buffer region independent of Reynolds number. This was also confirmed by the studies of Lindgren et al., (2004) in a high Reynolds number flow.

In the outer region, $p(u)$ deviates from a Gaussian distribution and the profiles are positively skewed due to intermittent nature of the flow. The flow in the outer part is characterized by large eddies that are three dimensional and elongated in streamwise direction (Blackwelder et al., 1972). The large structures form a wavy interface causing the non-Gaussian distribution of probability density distribution.

4.3.2 Near-wall perturbation

Figure 10 shows the variation of $p(u)$ for Series B. Each row represents the distribution at a given x/d station while each column shows the distribution at a given distance from the wall. At $x/d = 20$, the B-NP data are more negatively skewed compared to the reference profile (B-SM). At $x/d = 40$ and 60 , $P(u)$ for both B-NP and B-SM are equally negatively skewed in the near-wall region. As we move farther away from the bed (at $x/d = 20, 40$ and 60), in the overlap region, the probability density distributions for B-NP and B-SM are very close to Gaussian distribution. As indicated earlier, in the log-region, one would expect intense mixing and momentum exchange to result in the occurrence of a normally distributed probability density distribution. As we move further away from the wall into the outer region, the probability density distribution starts to deviate from Gaussian distribution and the profiles are positively skewed

4.3.3 Background Turbulence

The $P(u)$ for High-Tu and Low-Tu are plotted for various values of y^+ in Figure 11. The results conform to earlier discussion and no distinct background turbulence effects can be noticed in the present data.

4.4 Gram-Charlier expansion

Kampe de Fariet (1966) and others have suggested to study the dynamics of turbulence by investigating the degree to which the probability density function departs from the Gaussian form. Various possibilities for constructing multidimensional probability density functions based on series expansions and proposed the Gram-Charlier series. Lindgren et al., (2004) applied Gram-Charlier expansion very close to the wall and at the outer edge of the boundary layer showed significant difference from the Gaussian distribution. The probability density function can be expanded into Gram-Charlier series as

$$p(x) = C_0 \phi(x) + \frac{C_1}{1} \phi'(x) + \frac{C_2}{2} \phi''(x) + \dots + \frac{C_n}{n!} \phi^n(x) \quad (5)$$

$$\phi^n(x) = (-1)^n H_n(x) \phi(x) \quad (6)$$

Here, $\phi(x)$ is the Gaussian probability density function and $H_n(x)$ is the Hermite function. The values of the coefficients are $C_0=1$, $C_1 = C_2 = 0$, $C_3 = -S$, and $C_4 = 3 - F$, where S and F are the skewness and flatness factors. The expansion can be truncated at $\phi^5(x)$ due to increasing uncertainties in the higher order moments. The coefficient C_5 is related to hyper skewness in the following manner (Lindgren et al., 2004):

$$C_5 = -H_5 + 10S, \quad (7)$$

Where, H_5 is hyper skewness and defined as:

$$H_5 = \frac{\sum_i^N (U_i - \bar{U})^5}{N\sigma^5} \quad (8)$$

4.4.1 Reynolds number effect

The coefficients $C_3 - C_5$ from the present study are plotted along with the experimental data of Tsuji and Nakamura (1999) in Figure 12. Close to the wall i.e., in the viscous sublayer, C_3 has a value of -0.7, where as the corresponding value of is $C_4 \approx 0.68$ (i.e. $F_u > 3$), is a manifestation of the intermittent bursting events that take place there. In near-wall region, the inrush phase of the bursting cycle brings in high velocity fluid from the outer layer. With increasing y^+ , the value of C_3 increases and changes sign in buffer region (at $y^+ \approx 12$) and is nearly constant in overlap region. The coefficient C_4 is also constant in overlap region. The values of coefficients in log-region are $C_3 \approx 0$ and $C_4 \approx -0.2$, i.e., skewness is almost zero and flatness is about 2.8. The entrainment of fluid from surrounding flow causes intermittent mixing, which results in significant momentum exchange. As noted earlier, this will cause probability density distribution to resemble to Gaussian distribution in the log-region. The present results agree well with previously obtained experimental results by Tsuji and Nakamura (1999) and Ferholz & Finley (1996).

Consistent with the wider overlap region at higher Re_θ noted in the mean profiles, there is tendency for the region of nearly constant C_3 and C_4 to increase with increasing Re_θ . The Reynolds number effect, if any, becomes more significant in the higher-order profiles. The present distribution of C_5 for OCF also agrees with previous studies TBL data. Clearly, there is significant similarity in the two flow fields.

4.4.2 Near-wall Perturbation

The Gram-Charlier coefficients downstream of the spheres at several axial stations are plotted in Figure 13. At $x/d = 20$, significant difference from the reference profile can be noticed in C_3 in the near-wall and the over-lap regions, and supports the fact that effect of near-wall disturbance penetrates deeper into the flow. C_3 varies systematically from a value of about -1 and crosses zero near $y^+ = 100$. Farther away from the wall, the C_3 profile shows two peaks ($C_3 = 0.66$ at $y^+ = 207$ and $C_3 = 0.7$ at $y^+ = 1141$) whereas, the reference profile has one peak ($C_3 = 0.7$ at $y^+ = 1118$). The value of C_3 starts to decrease as the free surface is approached. A similar trend in C_3 can be seen at $x/d = 40$. Nano and Tagawa (1987) point out that a change in sign in the skewness factor (or negative C_3) is an indication of the existence of coherent structures. One would thus expect large coherent structures both near the wall and near the edge of the boundary layer. At $x/d = 60$, the C_3 profile collapses reasonably well over the reference profile, but the two peak values still persist, representing the recovery of flow is not yet complete. The value of C_3 is close to zero for wider range of y^+ with increasing x/d . Rows 2 and 3 in Figure 13 shows the variation of C_4 and C_5 with increasing x/d . Differences between B-NP and B-SM profiles can be noticed at $x/d = 20$ which decreases with increasing x/d .

4.4.3 Background turbulence

The effect of turbulence on the Gram-Charlier coefficients are shown in Figure 14. The C_3 profiles for both the tests collapse well in the inner region, where as differences can be seen in outer region. In the case of C_4 and C_5 profiles, larger

deviations between the profiles can be noticed only in the outer region towards the free surface.

4.5 Power Law

4.5.1 Reynolds number effect

Power laws were sought for the present data by curve fitting the data and are shown in Figure 15. It is of interest to identify the extent to which (range of y^+) the power law fits the data and compare with log-law. To this end, the fits were also carried out for different ranges of y^+ . The goodness of fit (R^2) is also indicated in each of the graphs. The power law coefficient C shows an increasing trend with increasing Reynolds number, whereas α decreases with increasing Reynolds number. As indicated in the graphs, the value of C and α change slightly with the chosen range of y^+ . The table in Figure 15 clearly indicates the extent of fit in the log-region (as indicated by the l^+ value) that there is no added advantage in using the power law over the log-law.

4.5.2 Near-wall perturbation

Figure 16 shows the power law fits with and without the near-wall perturbation. The unperturbed flow resembles the typical smooth wall profile and is shown as a dashed line in the graphs. With near-wall perturbation, the power law constants change with distance and slowly recover with increasing x/d . It is also clear from the figures that the data fit the power law better than the log-law even with near-wall perturbation.

4.5.3 Background turbulence

Figure 17 shows the power law velocity profile fit to the data with high background turbulence. It can be clearly seen that the turbulence levels affect the value of C significantly.

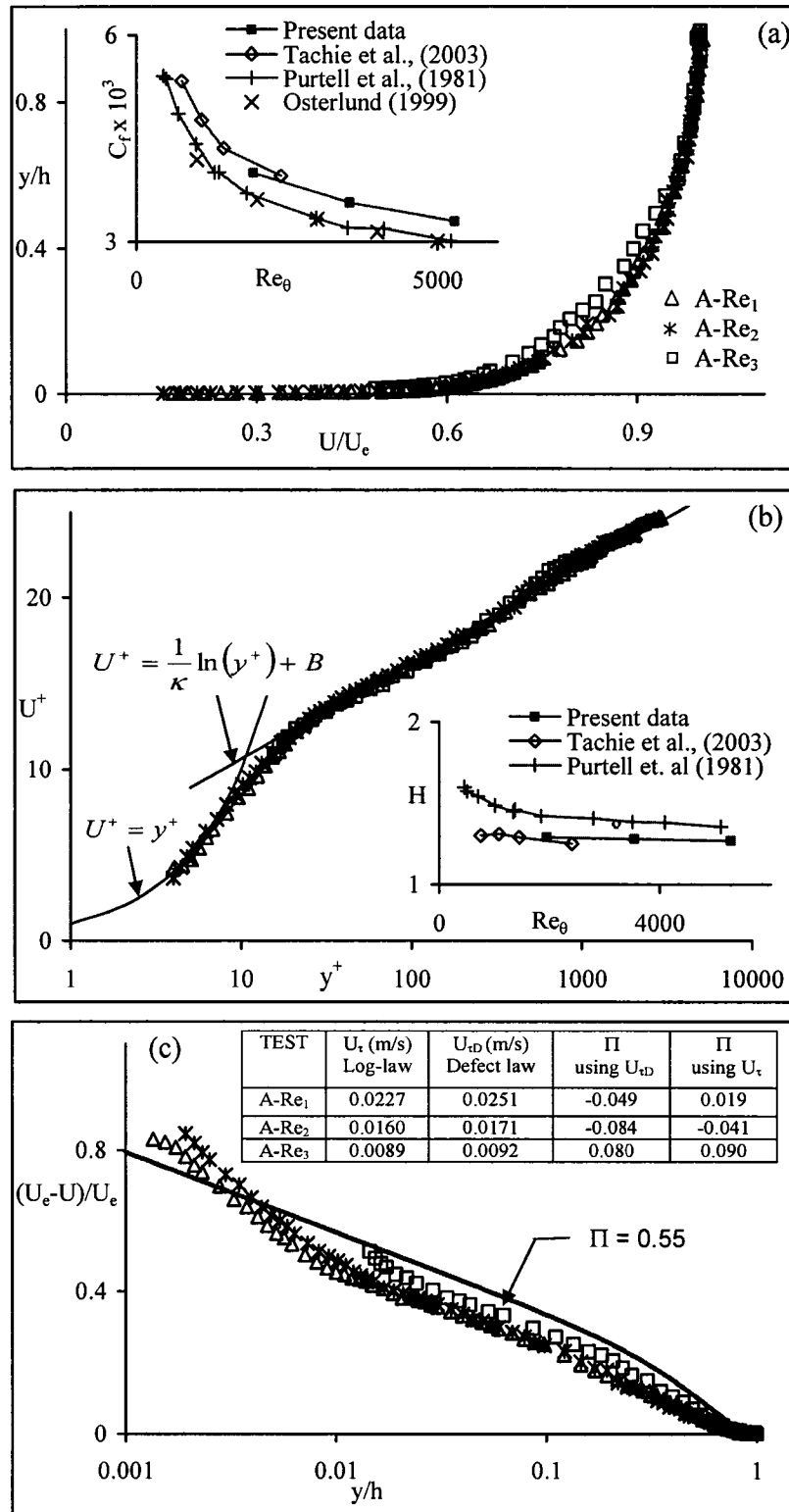


Figure 3: (a) Mean velocity profile in outer scaling & (b) inner scaling. (c) Velocity defect profile in outer scaling for various values of Reynolds number.

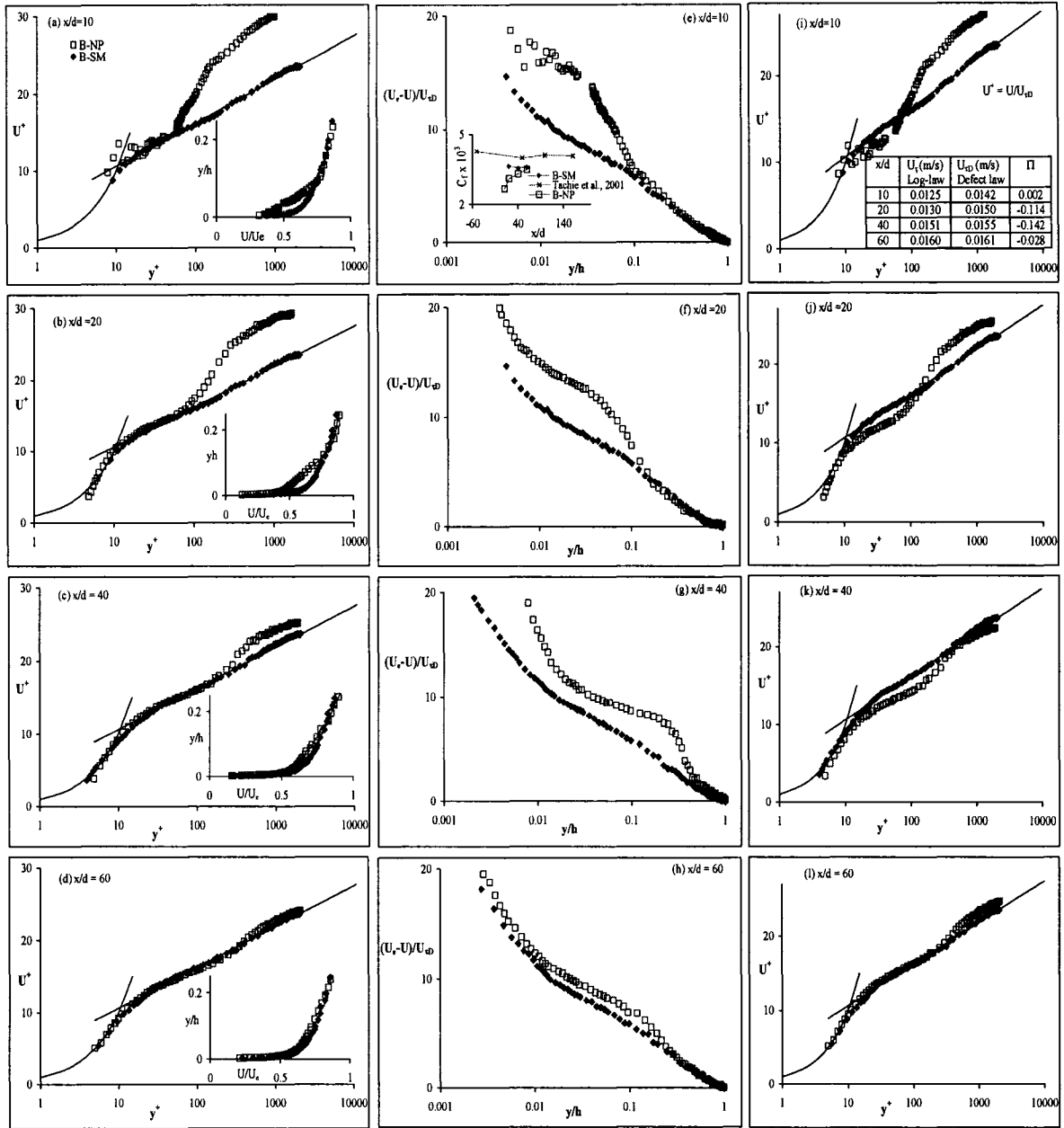


Figure 4: (a), (b), (c) & (d) Mean velocity profiles downstream near-wall perturbation and undisturbed flow at various locations inner scaling. (e), (f), (g) & (h) Mean velocity defect profile in inner scaling. (i), (j), (k) & (l) Mean velocity profile in inner scaling using friction velocity from defect law.

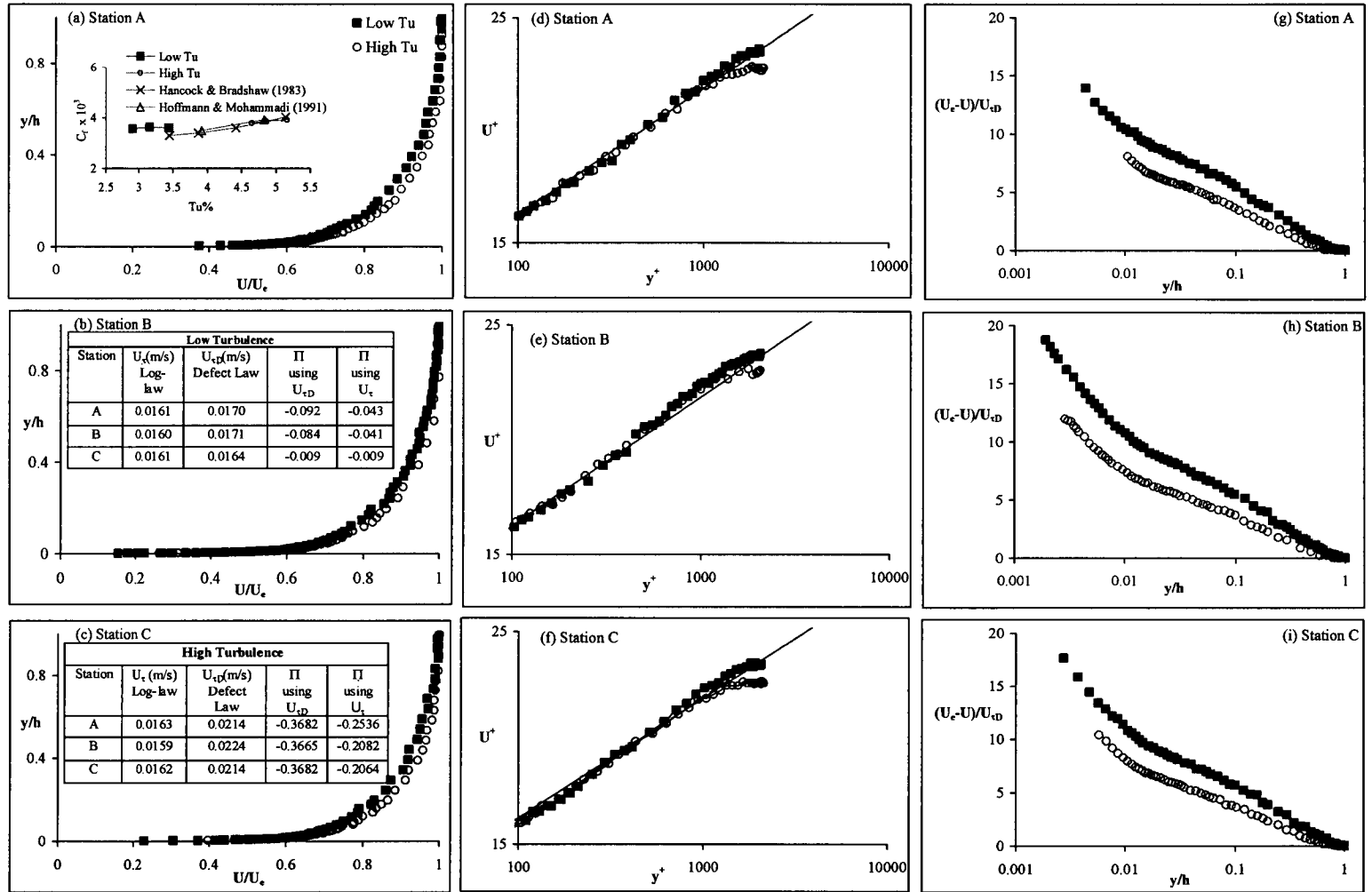


Figure 5: Mean velocity profiles for low and high background turbulence at various locations. (a), (b) & (c) outer scaling. (d), (e) & (f) inner scaling. (g), (h) & (i) Mean velocity defect profile.

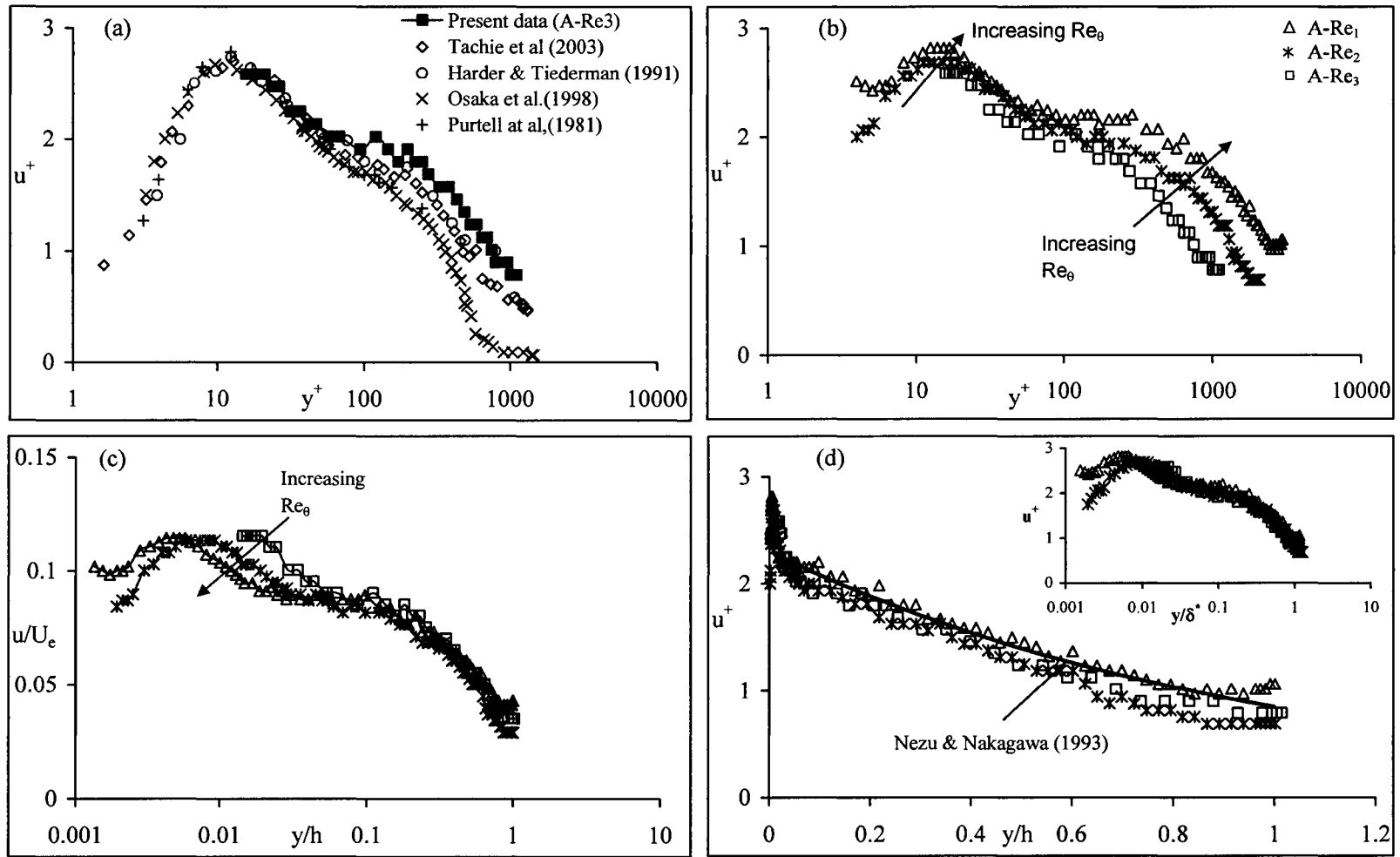


Figure 6: Distribution of Turbulence intensity in inner scaling for various values of Reynolds number (a) & (b) inner scaling (c) & (d) outer scaling.

43

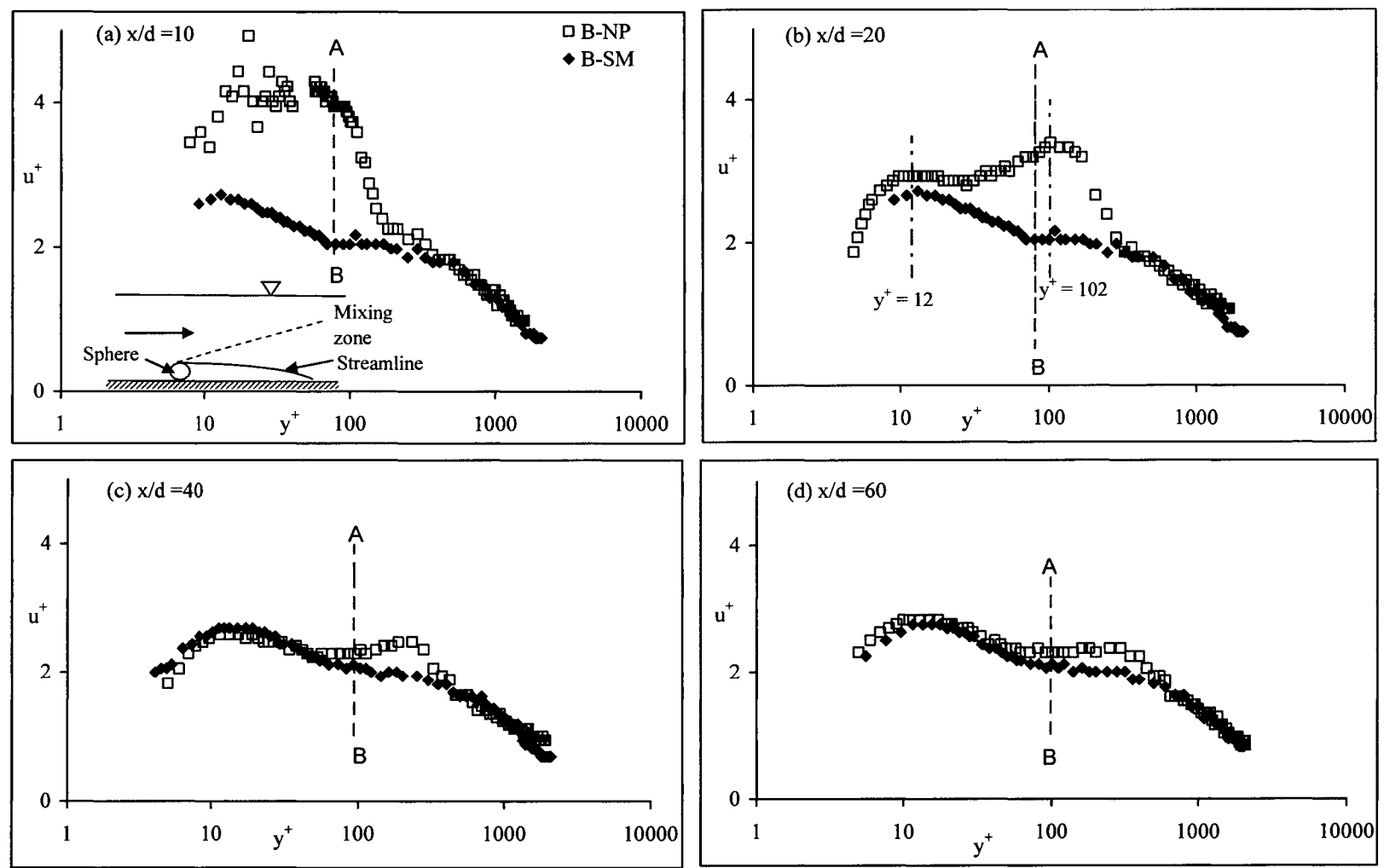


Figure 7: (a), (b), (c) & (d) Distribution of Turbulence intensity in inner scaling at various locations downstream of near-wall perturbation and undisturbed flow.

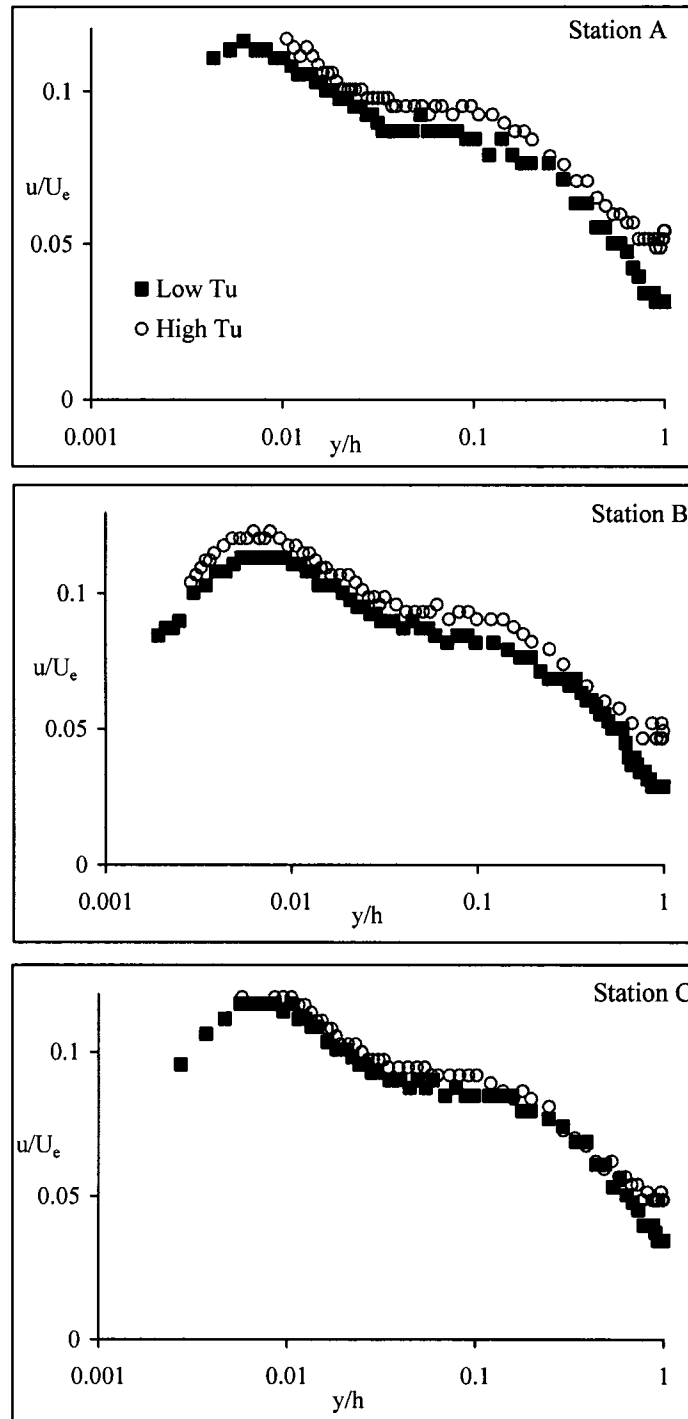


Figure 8: Distribution of Turbulence intensity for high and low background turbulence at various locations.

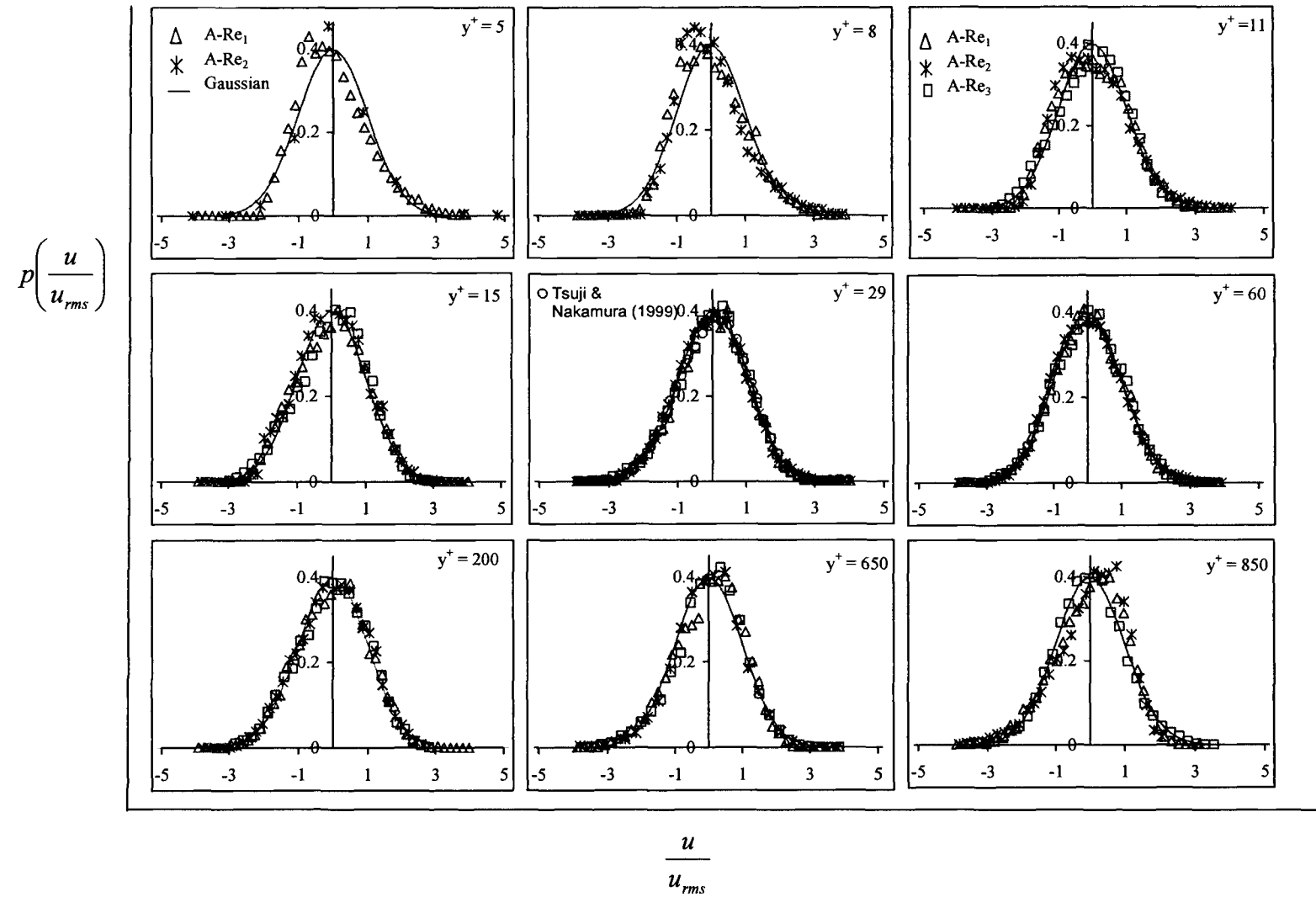
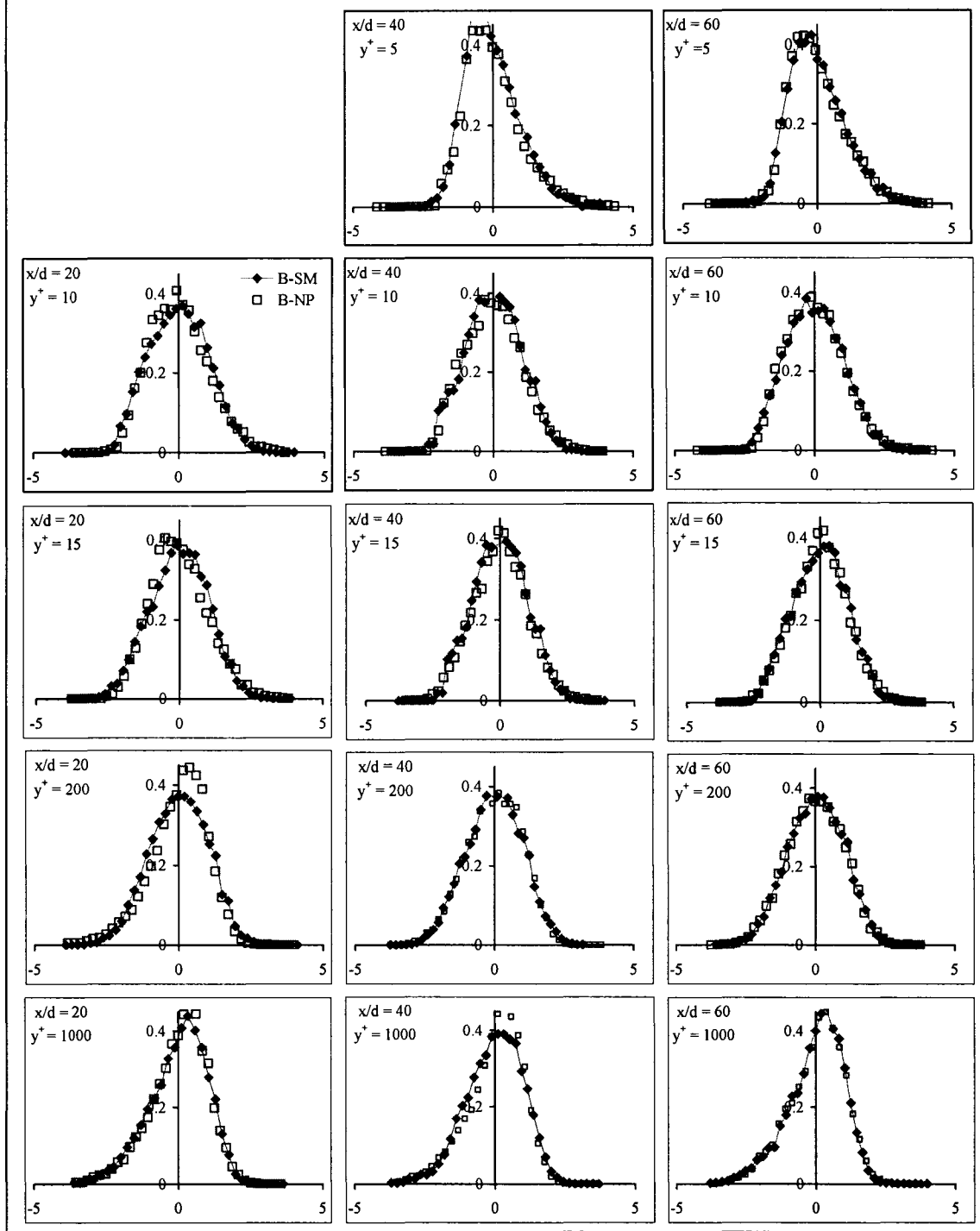


Figure 9: Probability density distribution of normalized u-component of velocity fluctuation for various values of Reynolds number.

$$P\left(\frac{u}{u_{rms}}\right)$$



$$\frac{u}{u_{rms}}$$

Figure 10: Probability density distribution of normalized u-component of velocity fluctuation downstream of near-wall perturbation and undisturbed flow.

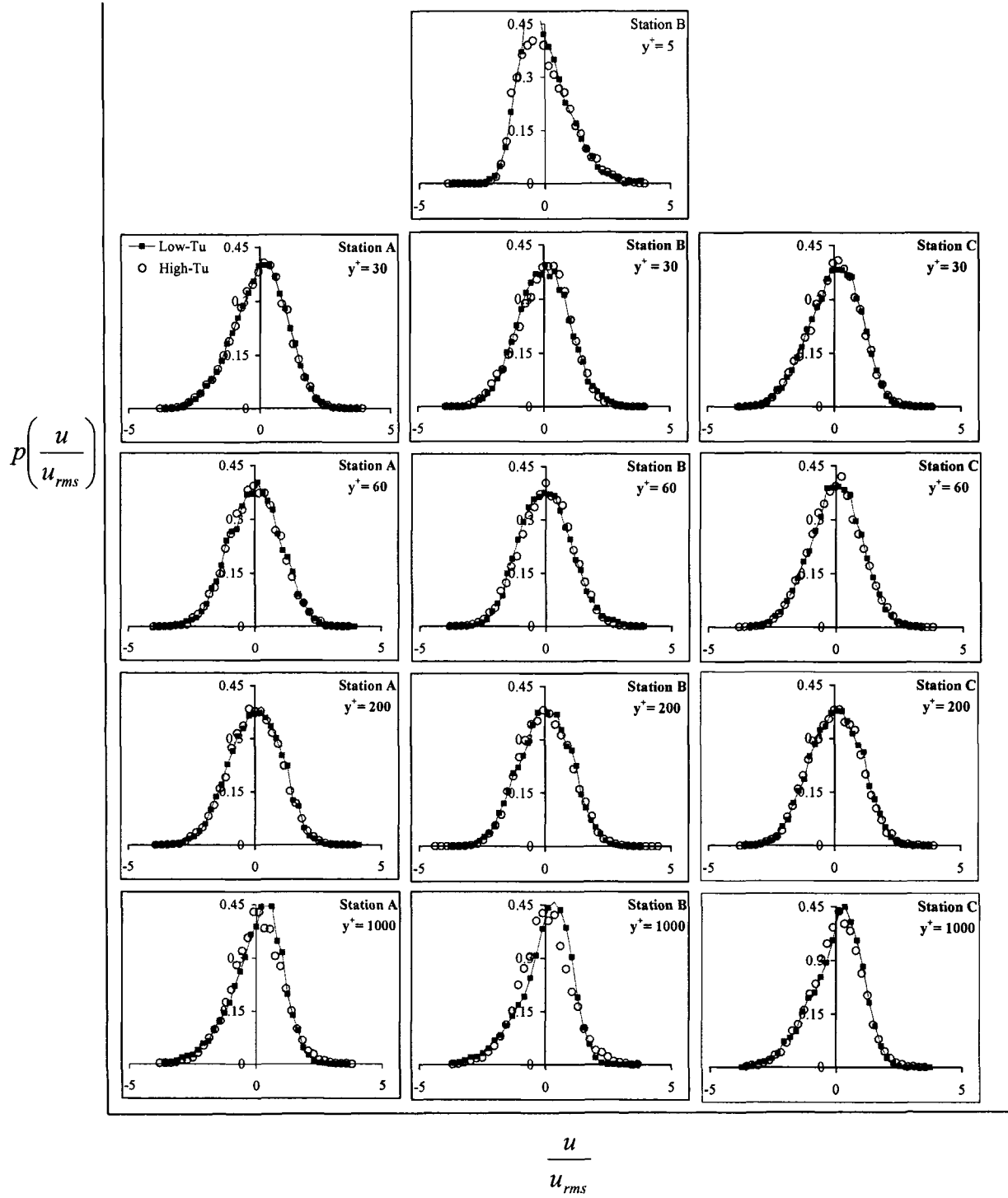


Figure 11: Probability density distribution of normalized u-component of velocity fluctuation for high and low background turbulence.

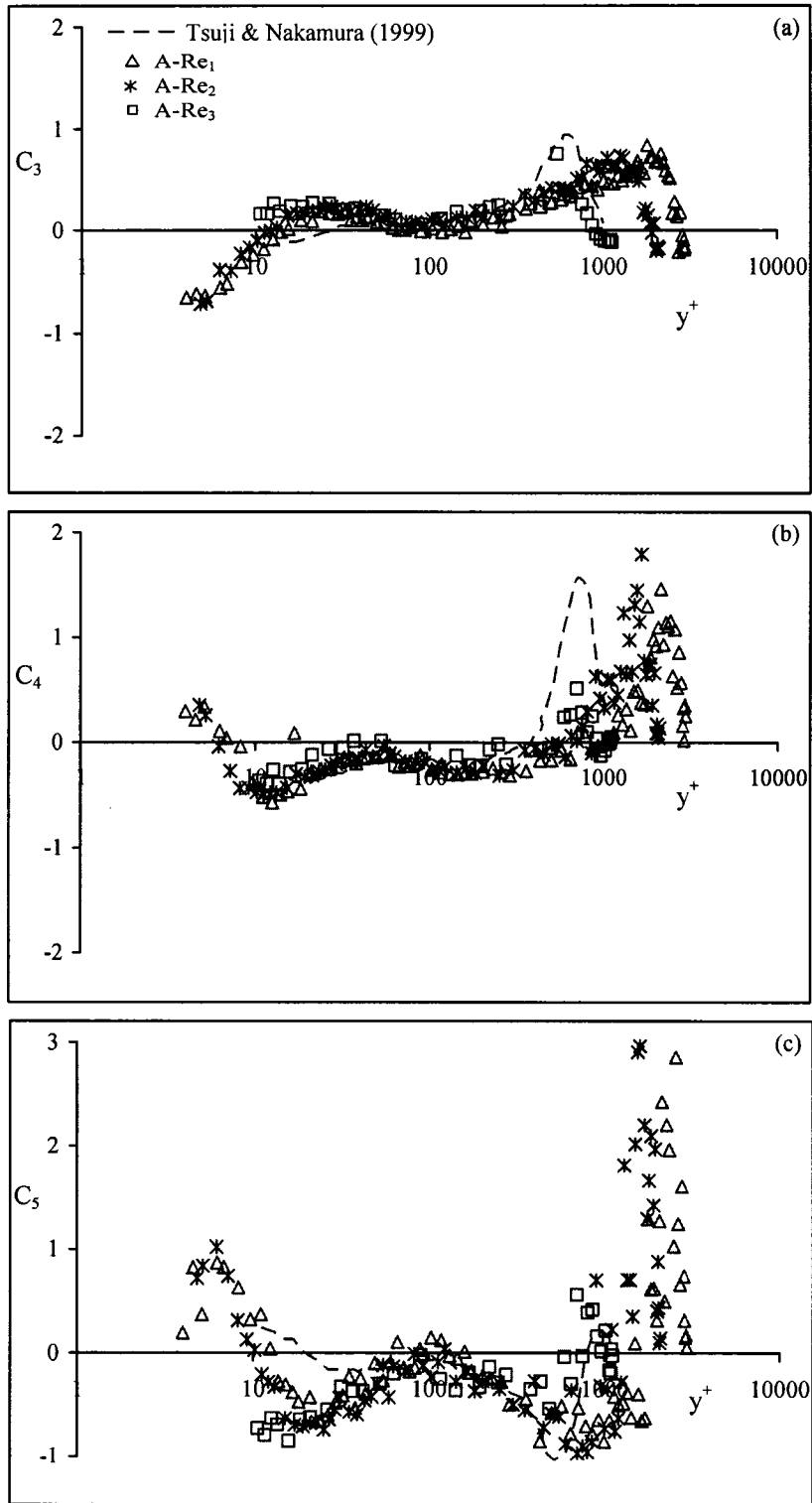


Figure 12: Coefficients of Gram-Charlier expansion for various values of Reynolds number

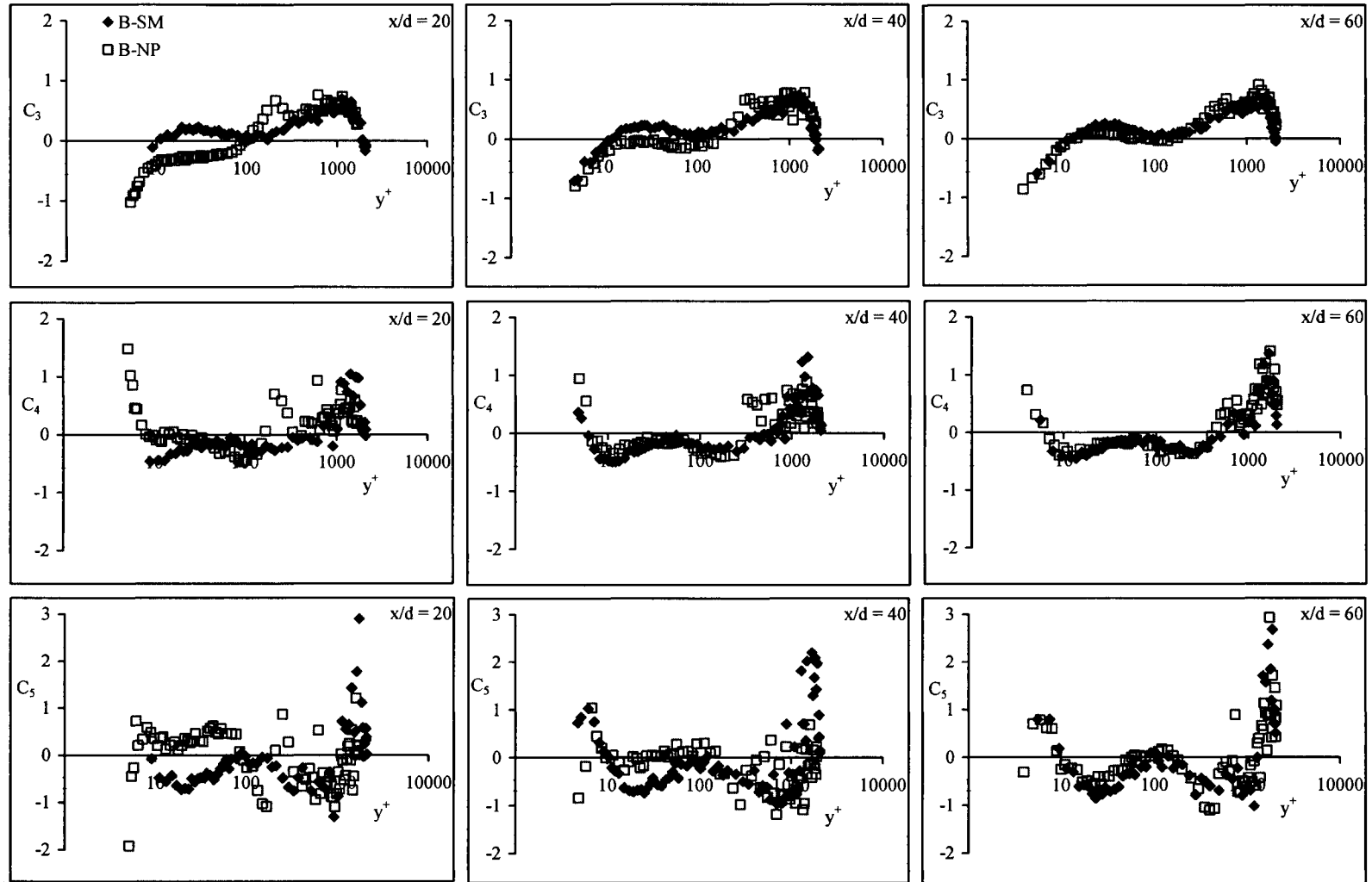


Figure 13: Coefficients of Gram-Charlier expansion series at various locations downstream of near-wall perturbation and undisturbed flow.

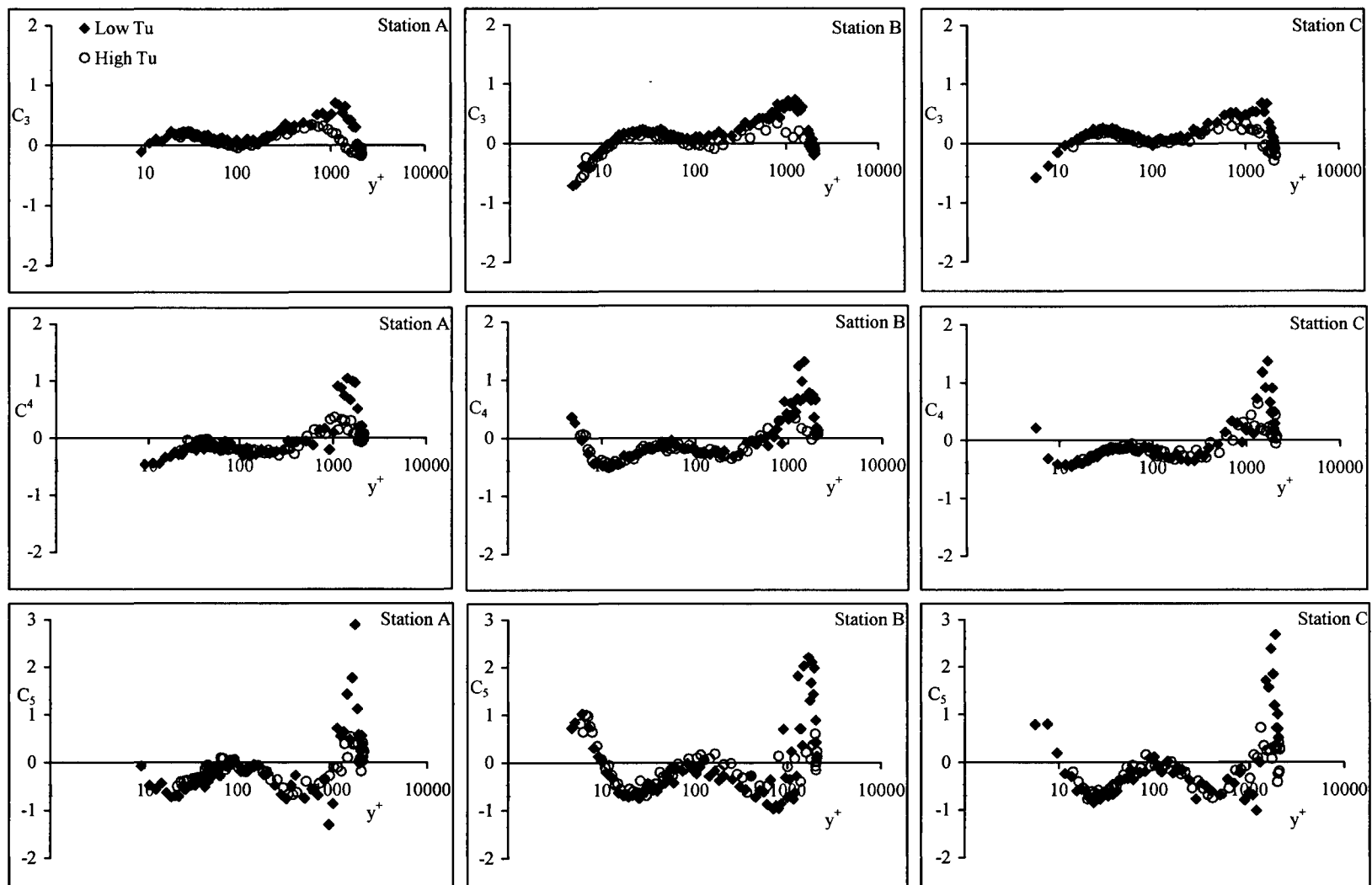


Figure 14: Coefficients of Gram-Charlier expansion series at various locations for high and low background turbulence.

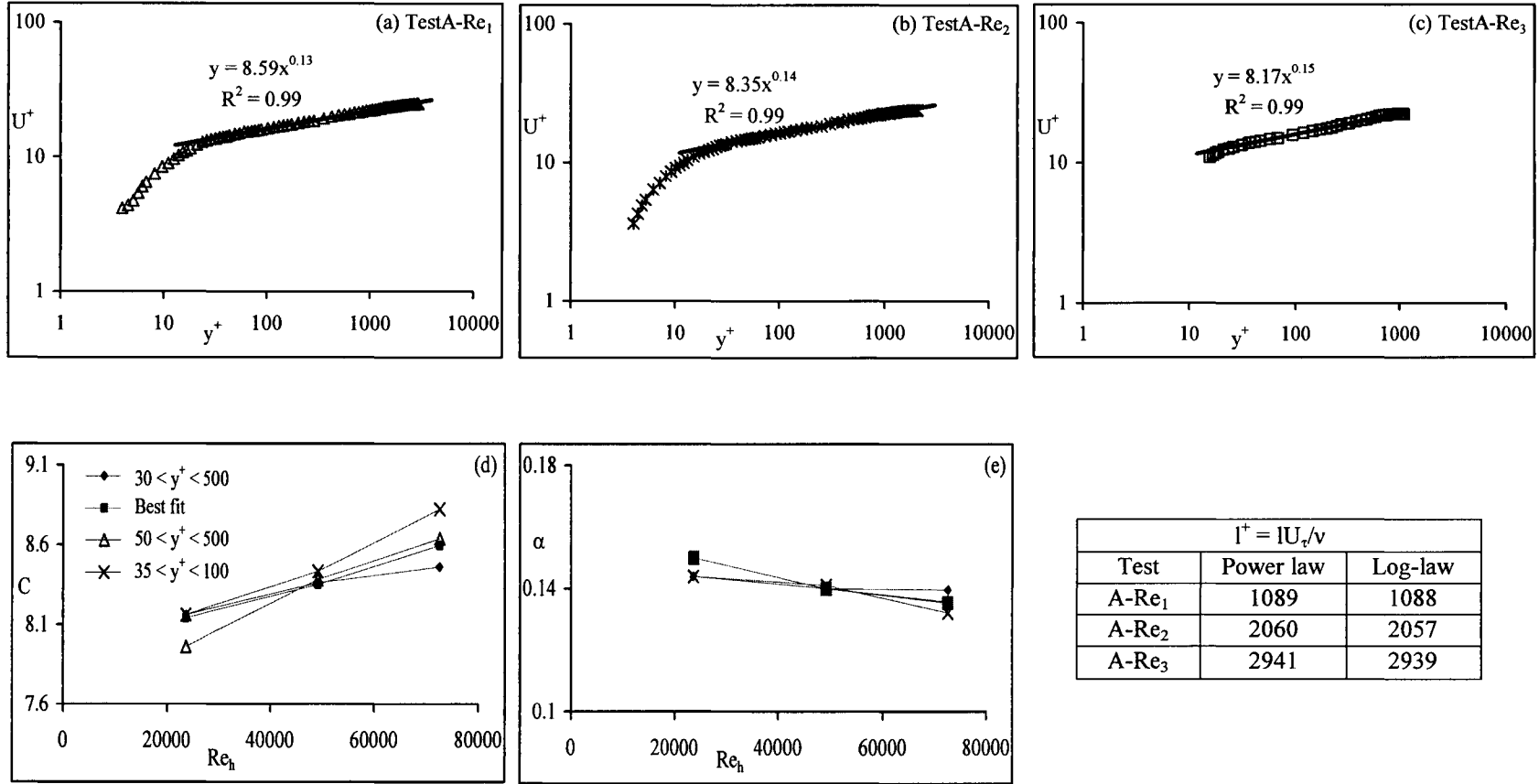


Figure 15: (a), (b) & (c) Power law Velocity profile for various values of Reynolds number. (d) & (e) Variation of Power law coefficients with Reynolds number based on depth of flow.

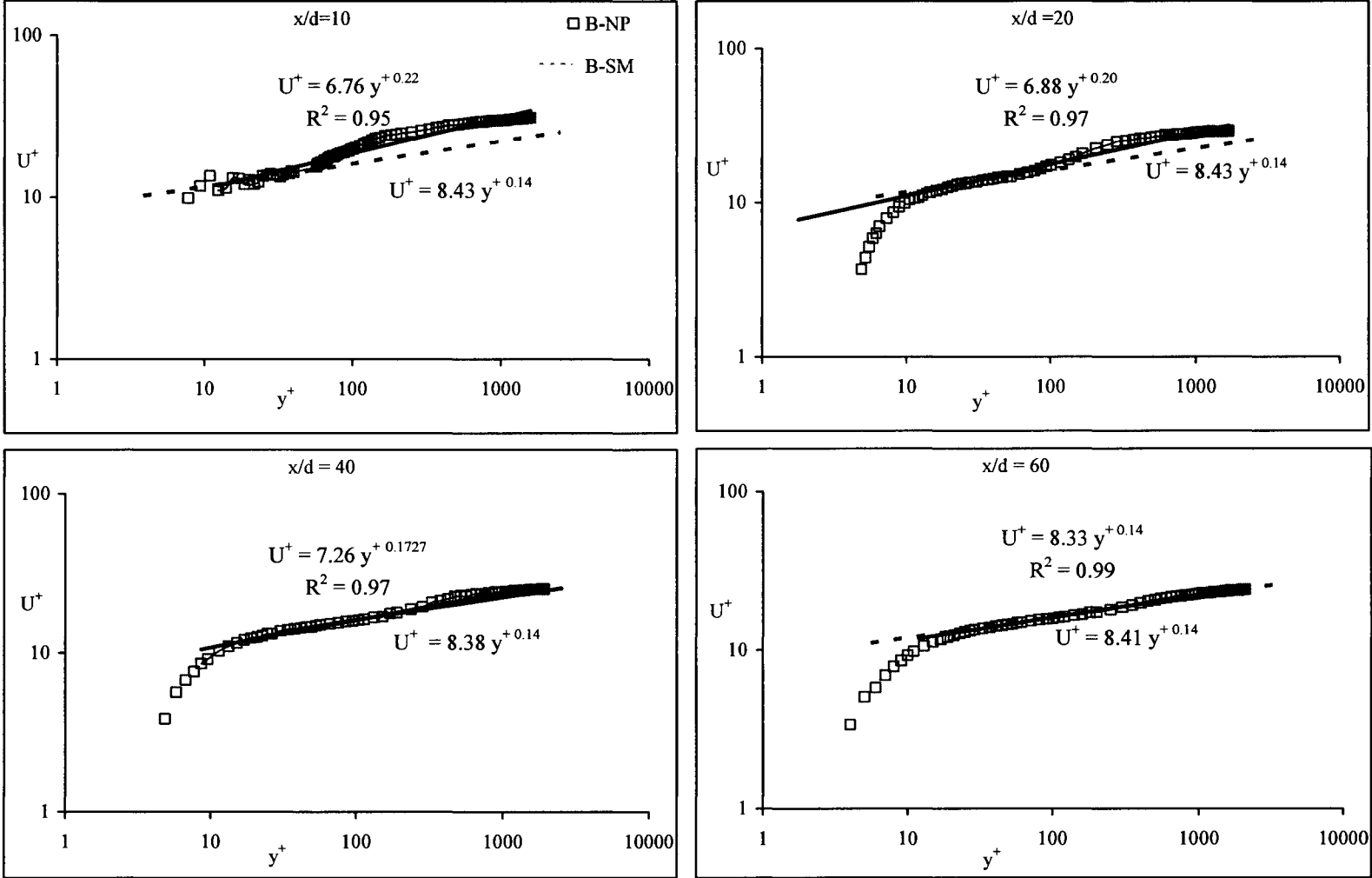


Figure 16: Power law velocity profile downstream of near-wall perturbation for undisturbed flow at various locations.

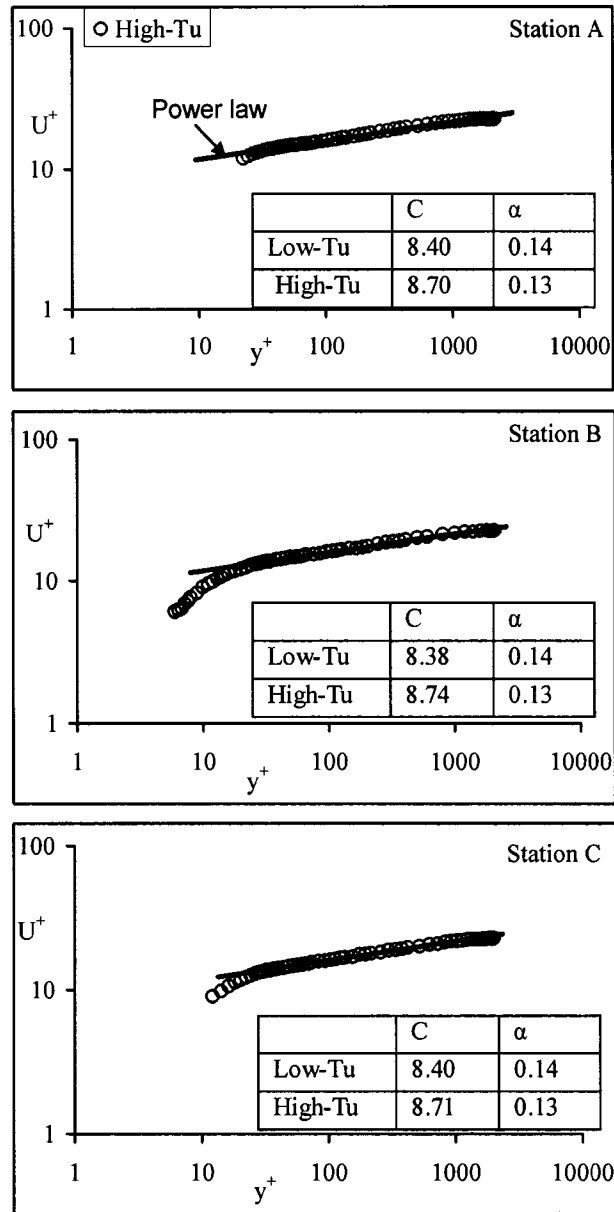


Figure 17: Power law velocity profile for low and high background turbulence at various locations.

CHAPTER 5

CONCLUSIONS AND RECOMMENDATIONS FOR FUTURE WORKS

5.1 Conclusions

In a smooth open channel flow, the mean velocity profile in inner variable showed that the extent of overlap or logarithmic region increased with increasing Reynolds number. The skin friction coefficient for the range of Re studied was higher than that noticed in canonical zero pressure gradients flows and decreased with increasing Reynolds number. The wake parameter of 0.55 obtained from zero-pressure gradient TBL was found to be inappropriate for the smooth OCF, and new values of wake parameters were determined. No definite trend can be established from the present study but the Π values are around zero. The present results support the fact that the overlap region exhibits Re dependence, irrespective of the scaling, however the scaling proposed by Roussinova (2006) reduces the Re effects. The probability density functions and the Gram-Charlier series coefficient distributions in OCF are very similar to that noticed in TBL.

The recovery of the flow was studied by observing the velocity profiles downstream of near-wall perturbation and compared with undisturbed flow. The results indicate that the profiles downstream of near-wall perturbation are quite distorted and the recovery of the flow to the undisturbed flow condition is slow. The present results do not show any significant differences in the mean velocity profile compared to the reference profile at $x/d = 60$. The mean velocity defect profile at $x/d = 60$ does not show recovery in the overlap region. The streamwise turbulence intensity profile showed two peaks

downstream of near-wall perturbation. The recovery of turbulence intensity in inner coordinates as well as outer coordinates is slower compared to mean flow. The agreement between the reference profile at $x/d=60$ can be seen in inner and outer region, where as in the overlap region turbulence intensity deviates from the reference profile. The $p(u)$ distributions close to the wall are more negatively skewed, compared with the reference profile. In the outer region, $p(u)$ deviates from a Gaussian distribution and the profiles are positively skewed. Observing the higher-order moments, differences can be seen in C_3 and C_4 from the reference profile in near-wall region as well as outer region, which shows that the effect of near-wall disturbance penetrates deep into the flow. At $x/d = 60$, C_3 , C_4 and C_5 do not collapse onto the reference profile. The coefficients of power law velocity profile showed recovery of flow at $x/d = 60$.

The presence of higher background turbulence significantly alters the characteristics of flow. Velocity defect in the outer region is decreased resulting in more negative values of the wake parameter, while the Gram-Charlier series coefficients are more uniformly distributed through the depth.

5.2 Recommendations for future works:

- 1) Since outer scaling and classical scaling does not absorb the effect of Reynolds number in overlap region. Therefore an intermediate scaling should be used for overlap region.
- 2) Application of very high resolution LDA is useful to explore the turbulence structure in the immediate vicinity of near-wall perturbation and also the free surface region of an open channel flow.
- 3) To further study the effect of size of the near-wall perturbation on the flow recovery.
- 4) To study the effect of background turbulence for various values of Reynolds number.

References:

- 1) Afzal, N. (2001). "Power law and log-law velocity profiles in fully developed turbulent boundary layer flow: Equivalent relations at large Reynolds numbers," *Acta Mech.*, 151, 195.
- 2) Andreopoulos, J., Durst, F., Zaric, Z., and Javonovic, J. (1984). "Influence of Reynolds number on characteristics of turbulent wall boundary layers," *Exp. Fluids.*, 2, 7–16.
- 3) Antonia, R. A., Bisset, D. K., and Browne, L.W. B. (1990). "Effect of Reynolds number on the topology of the organized motion in a turbulent boundary layer," *J. Fluid Mech.*, 213, 267–286.
- 4) Balachandar, R., Blakely, D., Tachie, M. F. and Putz, G. (2001). "A study of turbulent boundary layer on a smooth flat plate in an open channel," *J. Fluids Eng.*, 123, 394–400.
- 5) Balachandar, R., Blakely, D., and Bugg, J. (2002). "Friction velocity and power law velocity profile in smooth and rough shallow open channel flows," *Can. J. Civ. Eng.*, 29, 256-266.
- 6) Balachandar, R., and Ramachandran, S. (1999). "Turbulent boundary layers in low Reynolds number shallow open channel flows," *J. Fluids Eng.*, 121, 684–689.
- 7) Balachandar, R., and Tachie, M. (2001). "A study of boundary layer wake interaction in shallow Open channel Flows," *Exp. in Fluids.*, 30(5), 511-525.
- 8) Balachandar, R. and Patel, V. C. (2002). "Rough wall boundary layers on a plate in an Open channel," *J. Hydr. Engrg. ASCE*, 128(10), 947-951.
- 9) Balachandar, R. and Patel, V.C. (2005). "Velocity measurements in a developed open channel flow in the presence of an upstream perturbation," *J. Hydr. Res.*, 43(3), 258-266.

- 10) Barenblatt, G. I. and Prostokishin, V. M. (1993). "Scaling laws for fully developed shear flows. 2. Processing of experimental data," *J. Fluid Mech.* 248, 521.
- 11) Barenblatt, G. I. (1993). "Scaling laws for fully developed shear flows. 1. Basic Hypothesis and analysis," *J. Fluid Mech.*, 248, 513.
- 12) Bergstrom, D.J., Tachie, M.F. and Balachandar, R. (2001). "Application of power laws to low Reynolds number boundary layers on smooth and rough surfaces," *Phys of Fluids.*, 13, 3277–3284.
- 13) Bradshaw, P. and Wong, F. W. (1972). "The reattachment and relaxation of turbulence Shear Layer," *J. Fluid Mech.*, 52, 113-135.
- 14) Bradshaw, P. (1978). *Topics in Applied Pyysics, Turbulence*. (ed. P. Bradshaw), 12, 2nd ed., New York, Springer-Verlag.
- 15) Bushnell, D. M. and McGinley, C. B. (1989). "Turbulence control in wall flows," *Annu. Rev. Fluid Mech.*, 21, 1-20.
- 16) Cardoso, A. H., Graf, W.H. and Gust, G. (1989). "Rough wall turbulent boundary Layer on a Plate in an Open Channel," *J. Hydraul. Eng. ASCE*, 128 (10), 947-951.
- 17) Cardoso, A. H., Graf, W. H., and Gust, G. (1989). "Uniform flow in a smooth open channel," *J. Hydr. Res.*, 27(5), 603-616.
- 18) Castro, I. P., and Epik, E. (1996). "Boundary Layer Relaxation after a Separated Region," *Exptl. Thermal Sc.*, 13, 338–348.
- 19) Castro, I. P. and Epik, E. (1998). "Boundary layer development after a separated Region," *J. Fluid Mech.*, 374, 91- 116.
- 20) Ching, C.Y., Djenidi, L. and Antonia, R. A. (1995). "Low-Reynolds-number effects in a turbulent boundary layer," *Exp in Fluids.*, 19, pp 61–68.

- 21) Clauser, F. H. (1956). "The turbulent boundary layer". *Adv. Appl. Mech.* (4) 1-51.
- 22) Cole, D. (1956). "The Law of the wake in the turbulent Boundary Layer," *J. Fluid Mech.*, 1, 191- 226.
- 23) Dinavahi, S., Breuer, K. and Sirovich, L. (1995). "Universality of probability density functions in turbulent channel flow," *Phys. of Fluids*, 7, 1122–1129.
- 24) Durst, F., Jovanovic, J. and Johansson, T. G. (1992). "On the statistical properties of truncated Gram–Charlier series expansions in turbulent wall-bounded flows," *Phys. of Fluids*, A 4, 118–126.
- 25) Durst, F., Fischer, M., Jovanovic, J., and Kikura, H., (1998). "Methods to set up and investigate low Reynolds number, fully developed turbulent plane channel flows," *J. Fluids Eng*, 120, 496–503.
- 26) Ferholz, H. H and Finely, P. J.(1996). "The incompressible zero pressure gradient turbulent boundary layer: an assessment of the data," *Prog. Aerospace Sci.*, 32, 245-311.
- 27) Gad-el-Hak, M. and Bandyopadhyay, P. R. (1994). "Reynolds number effects in wall-bounded turbulent flows," *Appl Mech. Rev*, 47, 307–365.
- 28) George, W. K. Castillo, L. (1997). "Zero pressure gradient turbulent boundary layer," *Appl. Mech. Rev.*, 50, 689–729.
- 29) Hancock, P. E. and Bradshaw, P. (1983). "Effect of free stream turbulence on turbulent boundary layers," *Tans. ASME J. Fluids Eng.*, 105, 284-289.
- 30) Hancock, P. E. and Bradshaw, P. (1989). "Turbulence structure of a boundary layer beneath a turbulent freestream," *J. Fluid Mech.*, 205, 45- 76.
- 31) Harder, K. J. and Tiederman, W. G. (1991). "Drag reduction and turbulent structure in two-dimensional channel flows," *Phil. Trans. R Soc. London*, A 336, 19–34.

- 32) Henkes, R. A. (1998). "Scaling of the turbulent boundary layer along a flat plate according to different turbulent models," *Int. J. Heat Fluid Flow*, 19, 338–347.
- 33) Hinze, J.O. (1959). *Turbulence* First Ed., McGraw-Hill.
- 34) Hoffman, J.A. and Mohammadi, K. (1991). "Velocity profiles for turbulent boundary layers under freestream turbulence," *J. Fluids Eng.*, 113(3), 399-404.
- 35) Johansson, A.V. and Alfredson, P. H. (1983). "Effects of imperfect spatial resolution on measurements of wall-bounded turbulent shear flow," *J. Fluid Mech.*, 137:411–423.
- 36) Jovic, S., and Driver, D. M. (1994). "Backward facing step measurements at low Reynolds number, $Re_h = 5000$," *NASA Tech. Mem.*, 108807.
- 37) Jung, Y. Y., and Se, J. B. (1992). "Redeveloping turbulent boundary layer in the backward facing step flow," *J. Fluids Eng.*, 114, 552-529.
- 38) Krampa-Morlu, F. and Balachandar, R. (2005). "Flow recovery in the wake of a suspended flat plate," *J. Hydraulic Research*.
- 39) Kampe de Fariet. (1966). "The Gram Charlier approximation of the normal law and the statistical description of a homogeneous turbulent flow near statistical description of a homogeneous turbulent flow near statistical equilibrium," *David Taylor Model basin Report* No. 2013, Naval Ship research and Development Centre, Washington, DC.
- 40) Kim, J., Moin, P. and Moser, R. (1987). "Turbulence statistics in fully developed channel flow at low Reynolds number," *J. Fluid Mech.*, 177, 133–166.
- 41) Kirkgoz, M. S. and Ardichoglu, M. (1997). "Velocity profiles of developing and developed open channel flow," *J. Hydraul. Eng.*, 123(12), 1099-1105.
- 42) Kline, S. J. (1967). "The structure of turbulent boundary layers," *J. Fluid Mech.*, 30, 741.

- 43) Krogstad, P. A. Antonia, R. A. Browne, L. W. (1992). "Comparison between rough and smooth wall turbulent boundary layers," *J. Fluid Mech.* 245, 599–617.
- 44) Krogstad, P.A., and Antonia, R. A. (1999). "Surface roughness effects in turbulent boundary layers," *Exp. in Fluids.*, 27, 450–460.
- 45) Le, H., Moin, P., and Mahesh, K., (1997). "Direct numerical simulation of turbulent flow over a backward-facing step," *J. Fluid Mech.*, 330, 349–374.
- 46) Libby, P. (1996). *An introduction to turbulence*. Taylor and Francis Incorporated, Washington DC.
- 47) Lindgren, B. Johansson, A.V. Tsuji, Y. (2004). "Universality of probability density distributions in the overlap region in high Reynolds number turbulent boundary layers," *Phys. of Fluids.*, 16, 2587–2591.
- 48) Lu, S. S. and Willmarth, W. W. (1973). "Measurements of the structure of the Reynolds stress in a turbulent boundary layer," *J. Fluid Mech.*, 60, 481–571.
- 49) Nakagawa, H. and Nezu, I. (1977). "Prediction of the contributions to the Reynolds stress from bursting events in open-channel flows," *J. Fluid Mech.*, April , 80, part.1, 99-128.
- 50) Muste, M. and Patel, V. C. (1997), "Velocity profiles for particles and Liquid in open channel flow suspended sediment," *J. Hydraul. Eng.*, 123(9), 742-751.
- 51) Nezu, I. and Rodi, W. (1986). "Open-channel flow measurements with a laser Doppler anemometer," *J Hydr Eng.*, 112, 335–355.
- 52) Nezu, I. and Nakagawa, H. (1993). *Turbulence in open channel flows*, IAHR Monograph, A. A. Balkema, The Netherlands

- 53) Nezu, I. (2005). "Open channel Flow Turbulence and Its Research Prospect in the 21st Century," *J. Hydraul. Eng.*, 131(4), 229-246.
- 54) Osaka, H. Kameda, T. Mochizuki, S. (1998). "Re-examination of the Reynolds-number-effect on the mean flow quantities in a smooth wall turbulent boundary layer," *JSME Int. J Series B* 41, 123–129.
- 55) Osterlund, J. (1999). "Experimental studies of zero pressure-gradient turbulent boundary layer flow," PhD thesis, Royal Institute of Technology Department of Mechanics, Stockholm.
- 56) Osterlund, J., Johansson, A., Nagib, H. and Hites, M. (2000). A note on the overlap region in turbulent boundary layers," *Phys. Fluids* 12,1.
- 57) Purtell, L. P. Klebanoff, P. S. and Buckley, F. T. (1981). "Turbulent boundary layer at low Reynolds number," *Phys.of Fluids*, 24, 802–811.
- 58) Rashidi, M. and Banerjee, S. (1990). "The effect of boundary conditions and shear rate on streak formation and breakdown in turbulent channel flows," *Phys.of Fluids*, 2(10), 1827-1838.
- 59) Roussinova, V. Biswas, N. and Balachandar, R. (2006). "Revisiting turbulence in smooth uniform open channel flow," *J. Hydr. Res.*, (inPress)
- 60) Ruderich, R. and Fernholz, H. (1985). "An Experimental Investigation of a Turbulent Shear Flow with Separation, Reverse Flow, and Reattachment," *J. Fluid Mech.*, 163, 53–73.
- 61) Schlichting, H. (1979). *Boundary layer Theory* (7th ed). New York: McGraw-Hill.
- 62) Schwarz, A. C., Plesniak, M. W and Murthy, S. N. B (1999). "Turbulent boundary layers subjected to multiple strains," *Trans. ASM, J. Fluids Eng.*, 121, 526-632.

- 63) Smits, A. J. and Wood, D. H. (1985). "The response of Turbulent Boundary Layer to Sudden Perturbation," *Annu. Rev. Fluid Mech.*, 17, 321-358.
- 64) Spalart, P. R. (1988). "Direct simulation of a turbulent boundary layer up to $Re_h = 1410$," *J Fluid Mech.*, 187, 61-98.
- 65) Steffler, P. M., Rajaratnam, N. and Peterson, A. (1985). "LDA measurements in open channel," *J. Hydraul. Eng.*, ASCE 111, No. 1, 119-130.
- 66) Suksangpanomrung, A. (1999). "Investigation of unsteady separated flow and heat transfer using direct large eddy simulations," Ph.D dissertation, University of Victoria, Canada.
- 67) Tachie, M., Bergstrom, D. and Balachandar, R. (2000). "Rough wall turbulent boundary layers in shallow open channel flow," *J. Fluids Eng.*, 122, 533-541.
- 68) Tachie, M. F. (2001). "Open channel turbulent boundary layers and wall jets on rough surfaces" PhD thesis, University of Saskatchewan, Saskatoon.
- 69) Tachie, M., Balachandar, R. and Bergstrom, D. (2001). "Open Channel Boundary Layer Relaxation behind a Forward Facing Step at Low Reynolds Numbers," *J. Fluids Eng.*, 123, 539-544.
- 70) Tachie, M. F., Bergstrom, D. J., and Balachandar, R. (2003). "Low Reynolds number effects in open channel turbulent boundary layers," *Exp. Fluids.*, 34, 616-624.
- 71) Thole, K. A. and Bogard, D. (1996). "High freestream turbulence effects on turbulent boundary layers," *ASME J. Fluids Eng.*, 118, 276-284.
- 72) Tsuji, Y. and Nakamura, I. (1999). "Probability density functions in the log-law region of low-Reynolds number turbulent boundary layer," *Phys. of Fluids.*, 11, 647-658.

- 73) Tsuji, Y. Lindgren, B. Johansson, A. (2005). "Self Similarity of Probability density functions in zero pressure gradient turbulent boundary layers," *Fluid Dynamics Resh.*, 37, 293- 316.
- 74) Wei, T. and Willmarth, W. (1989). "Reynolds-number effects on the structure of a turbulent channel flow," *J Fluid Mech.*, 204, 57–96.

Uncertainty Analysis

This section contains the error estimation for the results reported in this study. The uncertainties in the mean measurements are quantified. The main source of error in the LDA measurements is the uncertainty in the determination of the frequency present in each burst of the processor. In addition to the above, the uncertainty in statistical quantities will also depend on the sample size (N).

A methodology for estimating uncertainty in LDA measurements was developed by Yanta and Smith (1973) and Schwarz et al., (1999). They derived the following relations for the uncertainty in the streamwise component of the mean velocity respectively:

$$\frac{\sigma_U}{U} = \left[(\sigma_o)^2 + \frac{1}{N} \left(\frac{u}{U} \right)^2 \right]^{1/2} \quad \text{Eq. (a)}$$

Where σ_o is the error due to the uncertainty in the determination of the beam crossing angle and N is the number of samples.

The corresponding expression for the streamwise component of the turbulence fluctuations is given by:

$$\frac{\sigma_u}{u} = \left[(\sigma_o)^2 \left(\frac{\langle uv \rangle}{u^2} \right) + \frac{1}{2N} \right]^{1/2} \quad \text{Eq. (b)}$$

Following Schwaz et al., (1999) a value of $\sigma_o = 0.4$ is adopted in the present analysis.

Typical estimates of uncertainties for the mean and fluctuation quantities are given in Table A using the test condition for Test A-Re₂.

U (%)	u (%)
0.4	0.6

Table A.1 Typical uncertainty estimates for Test A-Re₂

VITA AUCTORIS

Bushra Afzal was born in 1978 in Uttar Pradesh, INDIA. She graduated from Aligarh Muslim University, Aligarh, INDIA in 2000 with a Bachelor of Technology in Civil Engineering. She was accepted in the Faculty of Graduate Studies and Research at the University of Windsor in 2004 leading to the degree of Master of Applied Science in Civil Engineering.